A Theoretical Model of the Cornea as a Thin Shell of Variable Thickness in Relation to Radial Keratotomy

by

Sharon Lee Williams

submitted to the Faculty of the

Virginia Polytechnic Institute and State University

in partial fulfillment of the requirements for the degree of

Master of Science

in

Engineering Mechanics

APPROVED:

Wallace Grant, Chairman	Daniel Drysdale
Micheal W. Hyer	Daniel J. Schneck

June 1984

Blacksburg, Virginia

A Theoretical Model of the Cornea as a Thin Shell of Variable Thickness in Relation to Radial Keratotomy

by

Sharon Lee Williams

(ABSTRACT)

A theoretical study of the deformation fields of the cornea under internal pressure is presented. The general elasticity equations describing a thin shell of variable thickness are solved using finite difference techniques. To gain insight into the natural corneal structure, the constant thickness case is compared to one of normal thickness. The bending stresses are found to influence the cornea's natural curvature. In the third case, the normal thickness is increased 10% to model the edematous state resulting from the incisions made during radial keratotomy. A comparison of the third case reveals the increased thickness in the peripheral cornea makes a minor contribution to the displacement; but moreover, the curvature change is opposite to that desired from radial keratotomy. The incisions are necessary to weaken the lateral support of the shell allowing the displacement and change in curvature which corrects myopia.

ACKNOWLEDGEMENTS

Great appreciation is extended to Dr. Wallace Grant for his guidance and encouragement. Without his continuous efforts as an advisor, this thesis would not have been completed.

A special thanks goes to Dr. Daniel J. Schneck who provided direction throughout the author's academic career. It has been an privledge to study under both Dr. Grant and Dr. Schneck.

The opportunity is taken to acknowledge the remaining committee members: Dr. Michael W. Hyer, for his valuable and constructive advice, and Dr. Daniel Drysdale, for his commitment to ophthalmology. Dr. Daniel J. Frederick, C. William Smith, and Dr. George Swift were instrumental in defining the problem and the obstacles.

Warm thanks is given to Wanda K. Baber, for her time and sincere assistance in formatting the document.

The author is indebted to a devoted friend, Susan Shepard, whose wisdom in wording lent continuity to the development of the paper. Finally, the author would like to express her appreciation to her entire family, including Mr. & Mrs. James F. Boone, for their loving support and patience which makes the attainment of her ideals possible.

CONTENTS

1.0 Introduction 1

2.0 Anatomy and Physiology of the Cornea 6

2.1 Introduction 6

2.2 Anatomy and Structure 8

2.3 Physiology of Corneal Healing 21

2.4 Material Properties 24

3.0 Surgical Procedure 26

3.1 Development of Radial Keratotomy 26

3.2 Clinical Measurement and Evaluation 27

3.3 Summary of Operative Procedure 28

3.4 Complications and Results 29

3.5 Literature Review 32

4.0 Problem Definition 35

4.1 Introduction 35

4.2 Geometry 36

4.3 Equation Formulation 40

4.4 Boundary Conditions 45

5.0 Numerical Solution 48

5.1 Introduction 48

5.2 Finite Difference Analogs 48

5.3 Finite Difference Equations 49

5.4 Application of the Boundary Counditions to the Finite Difference Equations 51

5.5 Solution of the Finite Difference Equations 53

6.0 Results and Conclusions 56

6.1 Introduction 56

6.2 Comparison of a Constant Thickness and a Naturally Varying Thickness Shell 57

6.3 Results From Increasing the Natural Thickness of the Cornea . 64

6.4 Conclusions 72

A.0 Computer Code for Finite Difference Solution 74

Bibliography 80

Vita 85

LIST OF ILLUSTRATIONS

Figure 1. Frontal and Horizontal Views of the Radial Incisions . 4

Figure 2. A Meridional Cross-Section of the Eye Illustrating Its Major Structural Components. 7

Figure 3. A Cross-Section Across the Corneal Thickness Illustrating the Relation Between Each Layer 10

Figure 4. Illustration of the Difference in Structure of the Cornea and Sclera 14

Figure 5. Schematic Representation of the Proteoglycan Distribution from the Mid-Cornea to Sclera 17

Figure 6. Cross-Sectional Geometry 37

Figure 7. Resultant Forces and Moments Acting on a Spherical Element 41

Figure 8. Circumferential Normal Force, Axial Moment, and Circumferential Moment Distributions for Kraus' Numerical Example 55

Figure 9. Resultant Transverse Shear and Normal Force Distributions for a Cornea of Constant Thickness and of Normal Thickness 60

Figure 10. Resultant Bending Force Distributions for a Cornea of Constant Thickness and of Normal Thickness 61

Figure 11. Displacements and Deformed Shape of the Middle Surface in a Cornea of Constant Thickness and of Normal Thickness 62

Figure 12. Change in Curvature and Angle of Rotation for a Cornea of Constant Thickness and of Normal Thickness 63

Figure 13. Effective Shape of the Anterior Surface and Thickness Function for a Constant, Normal, and 10% Increased Normal Thickness 66

Figure 14. Resultant Transverse Shear and Normal Force Distribution for a Cornea of Normal Thickness and of a 10% Increase in Normal Thickness 67

Figure 15. Resulant Bending Force Distributions for a Cornea of Normal Thickness and of a 10% Increase in Normal Thickness 68

Figure 16. Change in Curvature and Angle of Rotation for a Cornea of Normal Thickness and of a 10% Increase in Normal Thickness 69

Figure 17. Displacements and Deformed Shape of the Middle Surface in a Cornea of Normal Thickness and of a 10% Increase in Normal Thickness 70

1.0 INTRODUCTION

Myopia, commonly referred to as nearsightedness, is a condition in which parallel rays entering the eye come to focus anterior to the retina.• The condition was first defined by Kepler in 1611. Analyzing the eye anatomically in 1632, Plempius reasoned myopia was due to the lengthening of the eye's axial diameter. Today the most widely known theory of axial lengthening is the eye's natural susceptibility to adapt to its environmental demands. The demands of reading increase with higher levels in cultural and technological development. Near work deforms the eye by requiring that it maintain a constant near focus. As the eye develops at an early age, the eye tends to retain its near-sighted focus. In agreement with this theory, myopia has been found to develop rapidly in teen-agers and stabilize at the age of 21 or 22.[9]

Once the development has stabilized, the patient has several alternatives: eyeglasses, contacts, keratomileusis, orthokeratology, and radial keratotomy. Usually used for far-sightedness, keratomileusis or "corneal changing" is a complicated surgical procedure in which the central portion of the cornea is sliced off, frozen, reshaped with a

---

• Anterior means toward the front of the eye as opposed to posterior meaning toward the rear of the eye.

lathe, and sewn back on. Another technique, orthokeratology, mechanically flattens the curvature of the cornea by wearing a successive series of hard contact lenses and may involve the use of a retainer. Keratomileusis and orthokeratology have met with varying degrees of success. Recently, opthalmologists view radial keratotomy, a relatively simple surgical procedure, as a more viable solution for those patients who are not satisfied with eyeglasses or contact lenses for either cosmetic or occupational reasons.[48]

Radial keratotomy is designed to correct low to moderate degrees of myopia. Ophthalmologists specify the appropriate range of vision as -2.00 to -8.00 diopters. A diopter is a unit of measurement corresponding to the inverse of the farthest distance at which the eye can properly focus. If a patient has four diopters of myopia, it means that the far point of vision is one-fourth of a meter from the eye. According to the Boston Framington Eye Study, approximately 70 million Americans, 33% of the population, are nearsighted. Of these 70 million, 10 million are in the range of -2.00 to -8.00 diopters.[47]

Keratotomy, derived from the prefix, kerato-, relating to the cornea and the root, -tomy, meaning a cutting operation, is defined as an incision through the cornea. When performing radial keratotomy, the surgeon makes eight radial incisions in the cornea extending from the central optical zone. The incisions do not interfere with the central field of

vision.[36] Figure 1 illustrates the frontal and horizontal views of the incisions. The frontal view looks similiar to the spokes of a wheel radiating from the central hub. The objective of the operation is to change the corneal curvature and move the focal point towards the retina. The incisions weaken the mechanical strength of the peripheral cornea allowing the intraocular pressure to deform the cornea, steepening the periphery and flattening the central portion.

The corneal deformation undergone after radial keratotomy is influenced by several factors: the incisions, themselves; an increase in thickness; and an internal change in the corneal material properties. The incisions cut the supporting structure of the cornea producing a discontinuity in the circumferential stress field. Once the incisions are made, the injuried tissue absorbs water and produces swelling. This process, called edema, alters the rigidity of the tissue by increasing the thickness and possibly changing its material properties.

The objective of this paper is to determine the contribution of an increase in thickness produced through edema to the deformation caused by radial keratotomy. In addition, the influence of normally varying thickness on the supporting capability of the corneal structure is examined.

A prior knowledge of the anatomy and physiology of the cornea is

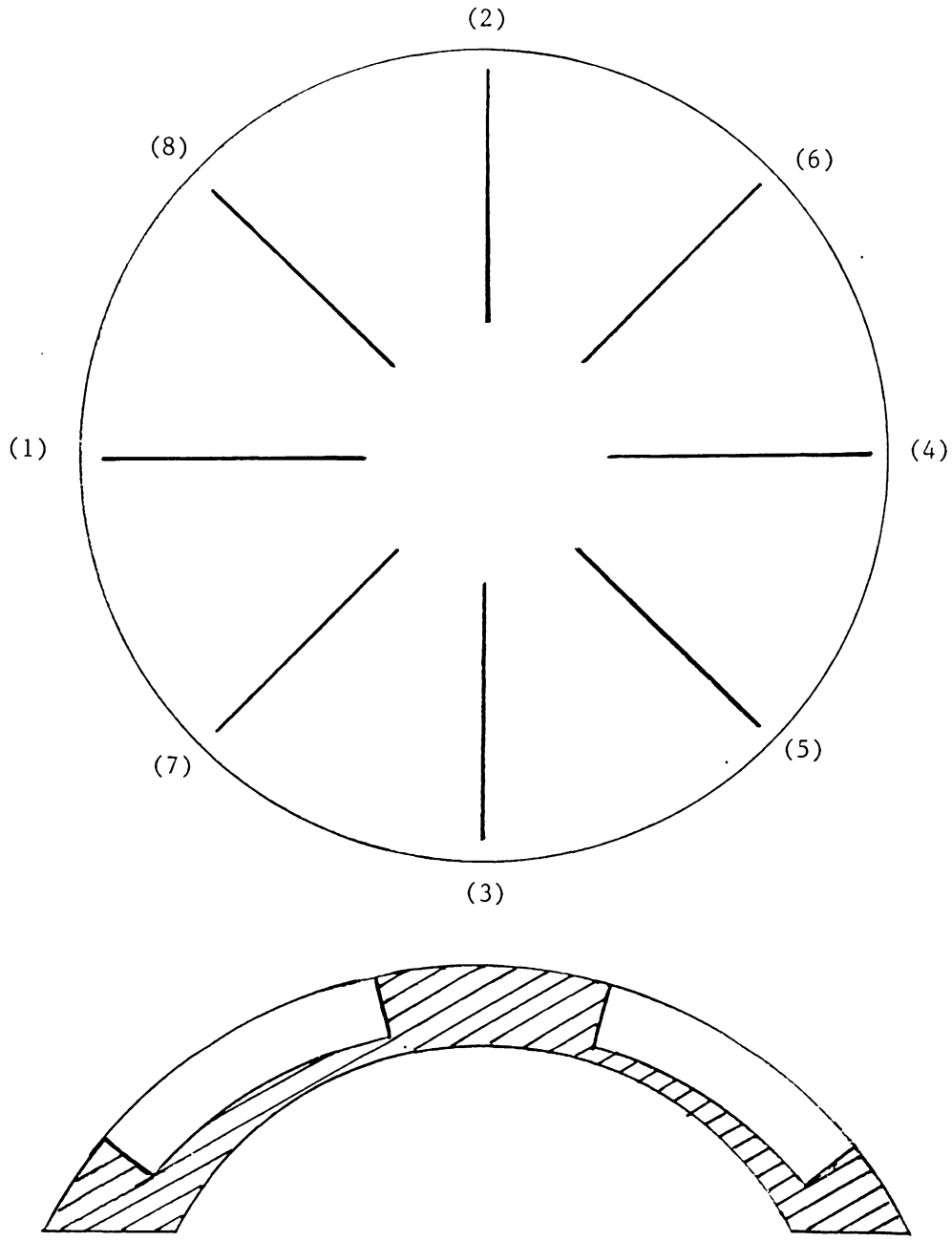

Figure 1. Frontal and Horizontal Views of the Radial Incisions: Note the order in which the incisions are made.

necessary in understanding its structural behavior in this problem. material properties. Chapter 3 summarizes the development, surgical technique, and complications of radial keratotomy. This chapter also includes the previous work done in analyzing the cornea as a shell structure. In the next chapter, the problem is defined with the formulation of the governing equations and boundary conditions describing the deformation of the cornea under internal pressure. The solution of these equations by finite difference techniques is discussed in Chapter 5. Finally, the results and conclusions are presented in Chapter 6.

2.0 ANATOMY AND PHYSIOLOGY OF THE CORNEA

2.1 INTRODUCTION

As illustrated in Figure 2, the eye is practically a hollow sphere filled with a transparent fluid, the aqueous humor. Within the sphere, the lens surrounded by the iris forms the anterior division which splits the eye into two chambers. The transparent portion of the shell, the cornea, and the lens serve a boundaries for the anterior chamber while the vitreous chamber is bounded by the lens and the retina. As light enters the eye, the cornea refracts it onto the lens which focuses the image on the retina. Converging to form the optic nerve, the nervous fibers of the retina receive light rays and transmit the visual signals to the brain for interpretation as visual perception.

The total refractive power of the eye's lens system is approximately 59 diopters, and of that total strength, the cornea provides nearly 44 diopters. In a simplified lens system, the cornea has two refractive interfaces: the interface between the air and anterior surface, and the interface between the posterior surface and the aqueous humor. The anterior surface is not uniformly curved but is approximately spherical and acts as a concave lens. Whereas the refractive index of the cornea is markedly different from that of the air, the anterior surface

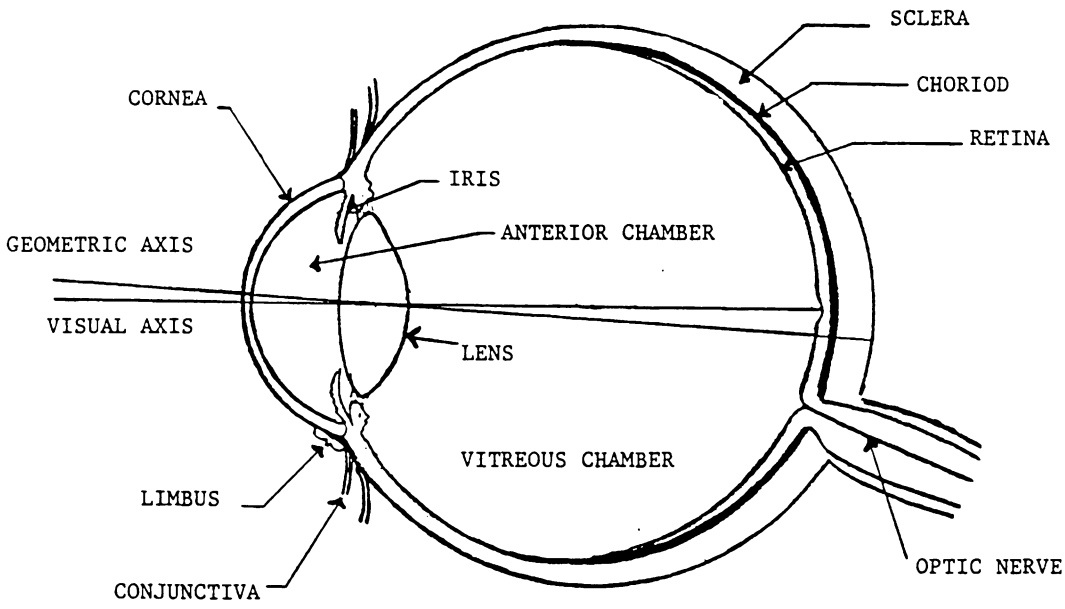

Figure 2. A Meridional Cross-Section of the Eye Illustrating Its Major Structural Components.

provides about 48 diopters in refractive power, while the more strongly This is due to the slight difference in refractive indices between the posterior surface and the aqueous humor.[17] With respect to the differing radii of curvature, 7.8 mm of the anterior surface and 6.6 mm of the posterior surface, the thickness of the cornea varies from 0.5 mm in the center to 0.66 mm as the periphery is approached.[7]

Other factors such as the structure and composition of the cornea influence its refractive properties. The next section deals with the anatomy and structure of the cornea as it relates to its transparency and material properties.

Since the investigation is of a surgical procedure, the third section discusses the physiology of corneal healing. The final section deals with the material properties of the cornea.

2.2 ANATOMY AND STRUCTURE

The protective envelope of the eye is a dense fibrous tunic which can be divided into two segments. The posterior segment, the sclera, forms nearly 5/6 of the outer envelope, and the more curved segment, the cornea, forms the anterior sixth of the outer coat. With the radius of curvature averaging 7.2 mm, the transparent membrane of the cornea

appears to be a section of a smaller sphere attached to the sclera, a larger sphere with a radius nearly 12 mm. At the sclerocorneal junction, the margin of the cornea overlapped with the sclera is defined as the limbus. In this region, circular fibers support the changing radii. The conjunctiva, the mucous membrane joining the anterior surface of the eye and the eyelids, begins at the sclerolimbal region.[7]

The cornea is composed of five layers:

1. Epithelium
2. Bowman's membrane
3. Stroma
4. Descemet's membrane
5. Endothelium.

(For identification of the layers, refer to Figure 3 for a cross-section across the corneal thickness.)

Epithelium

Covering the free surface of the cornea, the epithelium consists of 5-6 layers of cells with a total uniform thickness of 50-100 μ.[6] Structurally, the epithelium exhibits great regularity and is continuous

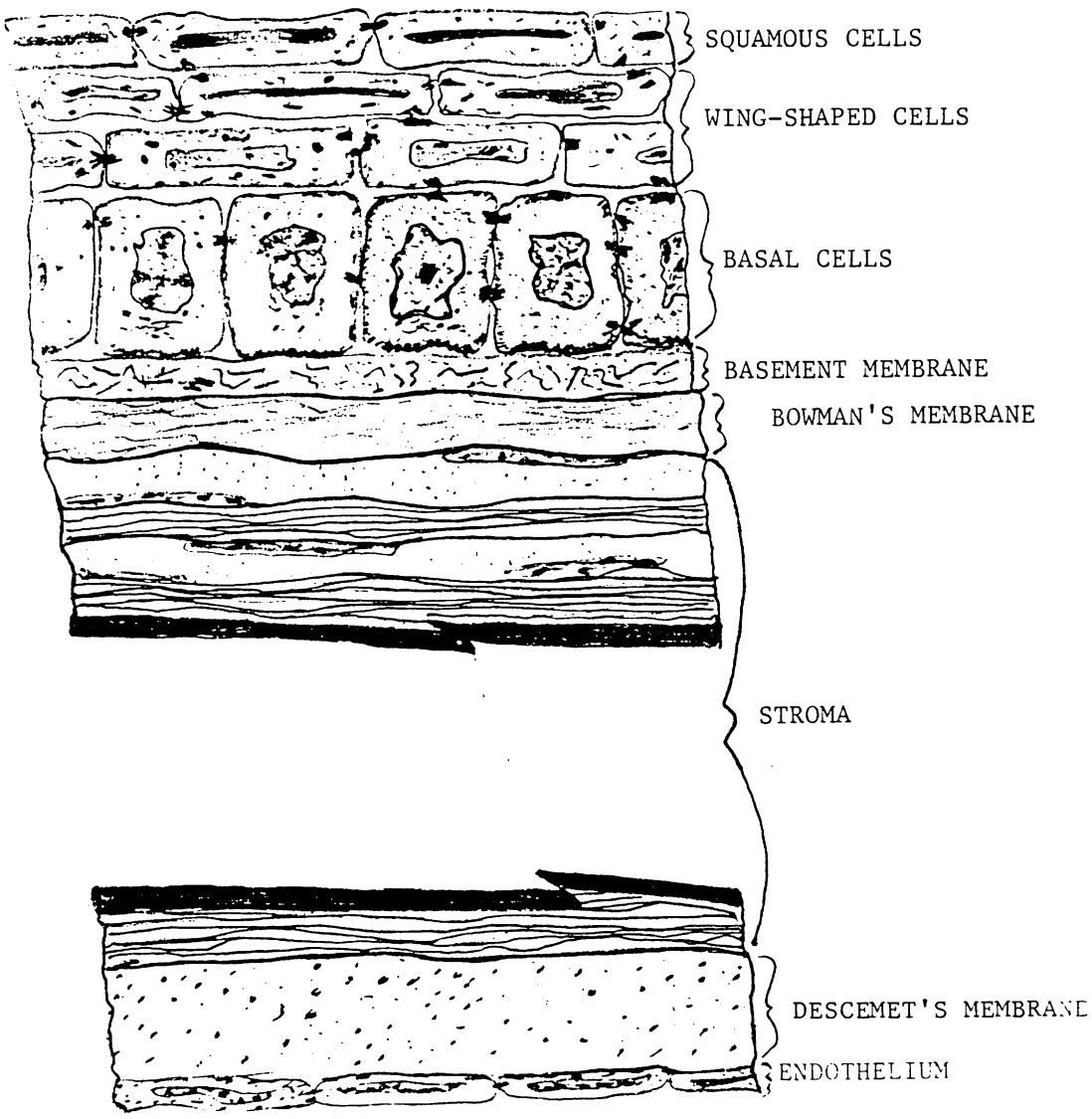

Figure 3. A Cross-Section Across the Corneal Thickness Illustrating the Relation Between Each Layer: (From Davson [6])

with the conjunctiva. The first two layers of the surface are squamous help hold the tear film in place, minute microvilli cover the surface of the squamous cells.[15] The next three layers are polyhedrical wing-shaped cells, convex on the anterior surface and concave on the posterior surface thus fitting onto the next layer. The last layer is a single row of basal cells, 18 μ in height and 10 μ in breath. These cells secrete the basement membrane, a thin layer that intervenes between the epithelium and connective tissue. The basement membrane is 10-30 μ thick and can be resolved into a lipid layer with a reticular fiber meshwork.[6]

The epithelial cells are bound together by desmosomes, an adhesive bridge between the cells. By joining the cells at the edges, these complex attachments prevent slippage and deformity. During corneal edema, the epithelial cells become separated except at the desmosomal attachments.[15] This creates an uneven surface which can not be smoothed by the precorneal tear film.[17]

The average life of an epithelial cell is 4-8 days and is replaced through mitotic division. Upon injury the epithelium undergoes rapid regeneration. Within 24 hours, a single cell layer is formed, and within several weeks, the epithelium is again 5-6 layers thick. The basement membrane is also reproduced after injury.[6]

Bowman's Membrane

Below the epithelium, Bowman's Membrane is 8-14 μ thick and ends abruptly at the limbus. There is no sharp difference between Bowman's membrane and the remainder of the stroma. Bowman's membrane simply appears to be a less ordered region of the stroma.[6] The consistency is similiar to the stroma; however, the load carrying collagen fibers, 100-150 A in diameter are closely but randomly packed.[15] The following section on the stroma will give a more detailed description of the collagen matrix configuration.

In no case is Bowman's membrane regenerated. Once an incision is made, a combination of epithelial slide and mitotic division fill the gap with epithelial cells. Some reparation is done by invading cells which deposit fibrous tissue, but the matrix never reaches its original thickness.[15]

Stroma

Approximately 90% of the corneal thickness, the stroma serves as the framework of the cornea. Collagen, the major portion of the thin connective tissue, provides the fibrous basis of the structure.[6] Constructed of a polymer of three polypeptide strands bonded in a

helical configuration, the basic structural units of the collagen fibrils form a highly ordered lattice.[30] The fibrils run parallel to each other and extend the full length of the cornea where they interweave with the scleral collagen as shown in Figure 4. The parallel fibers form bundles which also run parallel to the surface forming nearly 200 laminae.• Each lamina is 1.3-2.5 μ in thickness and 9-260 μ in width.[6] The laminae lay flat upon one another with almost no interweaving so that the layers slide easily over one another giving virtually no resistance in shear.[10] In each successive lamina, the fibers are essentially orthogonal to each adjacent layer. If the layers form right angles with each other, the normal stress in the principal direction of each ply should exhibit a maximum value; however experimentally, this does not appear.[35] Varying more or less at right angles to each other, the laminae of the collagen fibers form a fibrous composite cemented by a protein-mucopolysaccaride complex.

Flattened in the plane of the laminae lie the corneal corpuscles which function as fibrocytes, elongated cells which are usually present in connective tissue and capable of forming collagen fibers.[6] The corneal corpuscles, refered to as keratocytes, synthesize the bulk of the collagen and protein-mucopolysaccaride complex.[31]

• The laminae are referred to medically as lamallae.

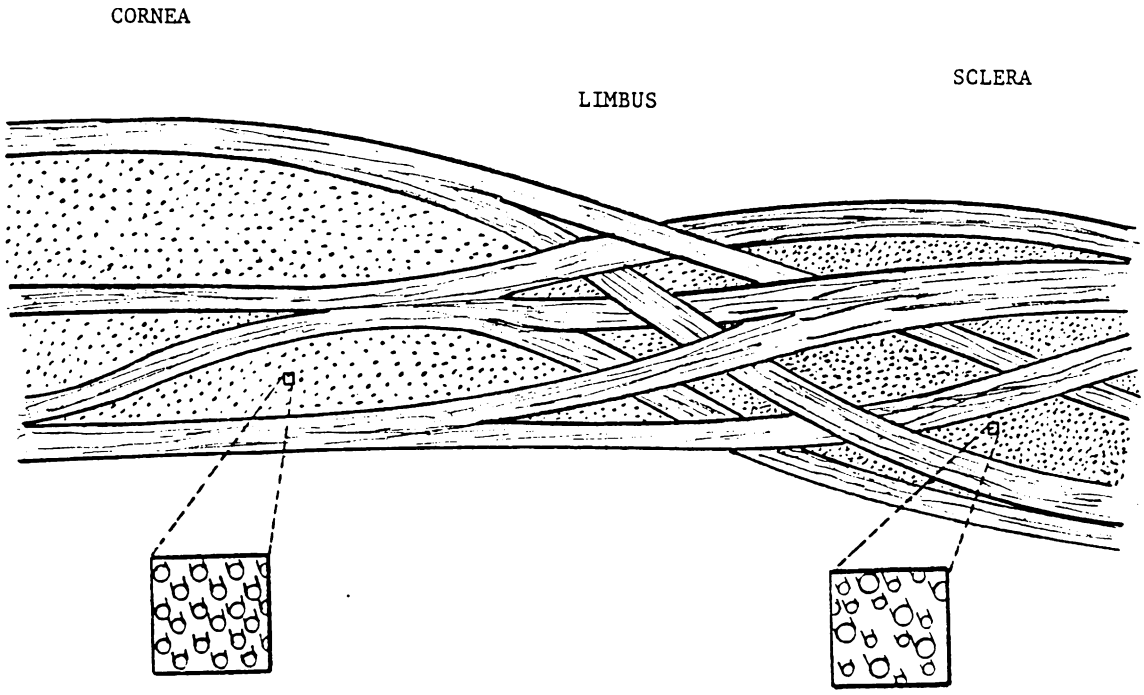

Figure 4. Illustration of the Difference in Structure of the Cornea and Sclera: Upon crossing the the limbus, the corneal laminae interweave with the scleral fibers. Note the difference in the regularity of the fiber diameter between the two tissues. (From Fatt [10])

The protein-mucopolysaccaride complex is commonly known as the ground term, proteoglycan, means that the polysaccaride component is the major portion of the complex and that the proteins are conjugated to the polysaccarides. The proteoglycans found in the cornea are keratan sulphate, dermatan sulphate, chrondroitin sulphate and its desulphated derivative, chrondroitin.[6] The highly negative proteoglycan chains arise from covalent bonds mainly to the serine and threonine amino acid segments of the protein core. The aggregrate is thus formed into linear polymers with closely spaced negative charges repelling each other to maintain a maximum distance between charged groups.[37] The aggregrate is oriented parallel to the collagen fibril with the protein core of the proteoglycan chains perpendicular to the long axis of the fibril, similiar to the bristles on a round brush.[13] Consequently, around each fibril, the proteoglycan aggregrate creates a negative field necessary to maintain the spatial separation between fibrils.

The cornea is the most rigorously parallel-fibered structure in the body.[14] The marked difference in uniformity and organization of the collagen between the cornea and the sclera can be correlated to the proteoglycan composition. Figure 5 illustrate the distribution of proteoglycans from the mid-cornea to the sclera. Only keratan sulphate and chrondroitin can be found at the central zone. The prescence of the highly negative keratan sulphate is sufficient to keep the spatial order

of the collagen. In the peripheral cornea, chrondroitin is replaced by the more negative chrondroitin sulphate. The combination of keratan sulphate and chrondroitin sulphate may account for the greater intrafiber distance in the periphery. At the limbus, keratan sulphate is replaced by dermatan sulphate. In the sclera, the aggregrate also associates with hyaluronic acid, a mucopolysaccaride that usually forms a gelatinous material in tissues spaces and acts as an intracellular cement.[13] There is a loss of uniformity in diameter, regularity in axial period, and order in the collagen lattice as the transition from keratan sulphate to the less negatively charged and more highly sulphated compounds begins in the limbus region.[31] The fibers in the cornea are homogeneous in diameter, 25-35 nm, with a characteristic axial period of 64 nm while the irregularly spaced scleral fibers vary in diameter from 28-260 nm with a wide range in axial period of 30-300 nm. In addition, the cornea is composed of 4.5% ground substance compared to 1% in the sclera.[10] Since the cornea differs from the sclera in a more negatively charged and greater concentration of proteoglycans, a higher ordered lattice is acheived in the cornea.

The corneal stroma has two separate indices of refraction for light polarized in different planes: the refractive index for collagen fibers is 1.55, and the index for the ground substance is 1.375. When light enters a material with two refractive indices, the light is refracted twice and split into two rays. Such a material is said to be

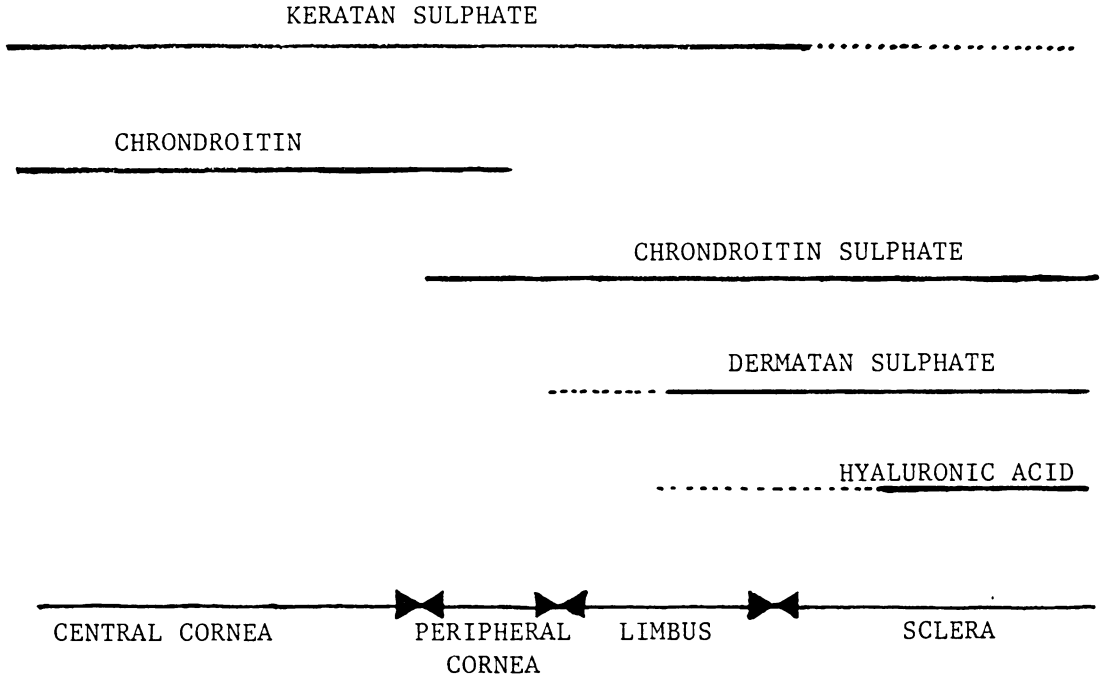

Figure 5. Schematic Representation of the Proteoglycan Distribution from the Mid-Cornea to Sclera: (From Davson [6])

birefringent, and the birefringence is defined to be the difference scatter light independently of one another, most of the incident light would be scattered; however, this is not the case. The diameter of the fibrils is greater than the wavelength of visible light, and accordingly, diffraction becomes important. Due to the regular spacing of the lattice, the diffracted rays passing forward tend to cancel each other by destructive interference. Since the light scattered by fibrils is destructive, the cornea appears transparent functioning as a complex diffraction grating.[10]

The cornea's transparency can be contrasted to the opaqueness of the sclera. The irregular spacing of the collagen fibrils causes the forward diffracted rays to no longer be cancelled by destructive interference. This forward scattering gives the sclera its characteristic appearance as the white of the eye.[10]

When the cornea swells, there is a change in the observed birefringence.[18] Swelling of the stroma results from the increased hydration of the matrix. Furthermore, this affinity to water is due to the presence of a large number of negatively charged proteoglycans.[13] Assuming all the incoming water goes into the matrix, swelling takes place only in the plane perpendicular to the surface. The arrangement of the fibers is distorted.[17] Moving the fibrils apart changes the

relationship between the fiber spacing and the wavelength of the light while the optical properties of the fibrils remain unchanged.[10] Edema causes the tissue to act as a diffraction grating so that light is broken into its component color appearing as a halo of surrounding light.[34]

Descemet's Membrane

Between the stroma and the endothelium lies a basement membrane secreted by the endothelium. Descemet's membrane is 5-10 μ thick[6] and thins as it approaches the limbus where it continues as the basement membrane of the scleral endothelium.[30]

The membrane's composition is different from the stromal composition. The characteristic polypeptide chains on the collagen molecules are not the same. The fibrils have an axial period of 117 nm as compared to 64 nm in the stromal fibrils. The membrane's collagen is similiar to the types found in the lens capsule and cartilage whereas the stromal collagen is similiar to the types found in the skin, bone, and tendon.[6]

When Descemet's membrane is cut, the elastic fibers retract curling up into a forward directed spiral. If the damage is done on the posterior surface of the cornea, endothelial cells migrate into the gap left by

the contracted fibers.[15] Should Descemet's membrane be perforated from the anterior side, stromal cells will migrate to the injuried site. Keratoblasts form a plug which becomes fibrous tissue in the large gap. The fibrous tissue shows no continuity with the endothelium.[8] Although the membrane is capable of regeneration by the endothelium, the cut edges never reunite.[15]

Endothelium

Covering the posterior surface of the cornea, the endothelium is formed by a single layer of large, flattened hexagonal cells about 5 μ high and 20 μ wide.[6] Microvilli cover the posterior surface greatly increasing the surface area.[15]

At first, the opthalmologists believed that the anterior and posterior surfaces were impermeable to water. These layers are now known to be permeable to water and salts.[10] The polysaccaride gel of the stroma has a tendency to take up water. As the fluid passively enters from the tears, the fluid must be pumped out of the cornea to maintain its thickness. The endothelial cells possess the ion pump necessary to extract the water bonded in the stroma and transport it into the anterior chamber.[13] The cells' role in the dehydration of the cornea and as a permeability barrier is of vital importance to the corneal tissue

and its clarity.[22]

Even though the endothelial cells have the ability to synthesize collagen and secrete Descemet's membrane, the endothelium cannot be regenerated. Mitotic division only occurs with growth and does not keep pace with the increase in surface area thus flattening the cells.[6] Progressive cell loss occurs with age; and furthermore, the loss is increased by cell damage through injury and disease. The endothelial cells are capable of compensating for a reduction in cell population by spreading out and enlarging three to four times their original size.[15] However, there is a limit at which the cell loss is too great for the new endothelium to support the full activity of the fluid pump. At this point the normal thickness of the cornea cannot be maintained; and consequently, the corneal clarity is compromised.[6]

2.3 PHYSIOLOGY OF CORNEAL HEALING

The cornea has no blood or lymphatic vessels. When a clean incision is made during radial keratotomy, the cornea heals in an avascular manner. If the wound was extensive, blood and lymphatic vessels would grow into the cornea to accelerate the healing process.[8]

The tissue reaction begins in the anterior stroma. As tears flow into the wound, edema rapidly spreads until reaching maximum opaqueness

within twenty-four hours.[8]

Following the influx of water, the epithelial cells infiltrate the wound forming a protective layer over the injured tissue. As the individual epithelial cells flatten, spread, and undergo mitotic division, the cells attempt to fill every crevice to make the surface smooth and regular again. The epithelial cells, particularly the basal cells, are believed to manufacture several chemical substances which initiate the assistance of the stromal cells.[8]

Within one hour, many stromal cells in the vicinity die losing their projections and synaptic pattern. In the surrounding areas, the cells proliferate and send out coarse projections.[15] Travelling through the laminae, these keratoblasts develop into long spindle cells resembling fibroblasts from which they were originally derived.[8] Once the damaged area is reached, these cells synthesize three mucoploysaccarides: keratan sulfate, chrondroitin, and chrondroitin sulfate.[15] Later, the stromal cells supplement the matrix synthesis with the formation of collagen fibrils.[8]

The cornea is first invaded by polymorphonuclear leucocytes, white blood cells. Initially, the cells escape the conjunctival vessels near the limbus, transverse the conjunctiva, and pass superficially to the wound by way of the tear film. Later the cells, migrating from the perilimbal

vessels, also travel through the laminae deformed into long spindle shapes. Crowding around the injuried area mainly under the epithelium, the leucocytes function as scavengers ingesting dead tissue, degenerated cells, bacteria, foriegn particles and the like. The phagocytic activity is well established within twenty-four hours and lasts for three to four days before the formation of collagen. The polymorphonuclear leucocytes begin to disappear in a week.[8]

Within fourty-eight hours, a second invasion of macrophages occurs. At first, the large ameboid mononuclear cells act as scavengers removing cellular debris but are later transformed into keratoblasts forming new collagen fibrils and corneal corpuscles.[15]

Cuts that are made along the meridian of the cornea become V-shaped gaps in cross-section due to the intraocular pressure. Bridging the gap, the keratoblasts are aligned perpendicular to the walls of the wound. The somewhat spindle shaped fibrils are deposited parallel to the elongated surface of the keratoblasts and are irregularly disposed in a reticular fashion running in non-parallel bundles. The courser regenerated fibrils do not have the same regularity in axial period as do the fibrils in the normal laminae, and the average diameter of the fibrils in the scar is much wider than that of the uninjuried tissue.[38] Accordingly, the regenerated matrix does not form a perfect optical medium.[8]

About fourty-five days into the healing process, the structure of fibrils becomes more regular, and the cells, originally plentiful under the epithelium, diminish in number.[8] Carrying the tension applied by the intraocular pressure, the fibrils tend to conform to the configuration of the normal laminae, and align perpendicular to the incision in order to contract the gaping margins of the wound.[15] By assuming this configuration, the collagen fibrils only support the tension applied normal to the incision. As the wound contracts, the thin hairline scars diminish in cloudiness; however, the ideal optical and mechanical state is not attained.

2.4 MATERIAL PROPERTIES

The cornea displays material properties characteristic of soft tissue. Its behavioral features include a non-linear stress-strain relationship under load-elongation, hysteresis in cyclic loading, stress relaxation at constant strain, creep at constant stress, and preconditioning in repeated cycles.[14]

To determine the rheological properties in the plane of the corneal surface, Nyquist performed uniaxial tension tests on the tissue. After observing the non-linear stress-strain relationship, he concluded that for small stresses in the physiologic range, the mechanical properties are nearly linear whereas at higher stresses, the non-linear

characteristics predominate.[35] Kobayashi and Larson's uniaxial tension tests were in quantitative agreement with Nyquist's data.[23]

Based upon Nyquist's work, the viscoelastic cornea is simplified to behave as a Hookean elastic solid in the physiologic range of stress. From his data, an acceptible value for Young's modulus, E, is 4.86×10^7 dynes/cm^2.

Due to its large water content, the cornea behaves similiar to most biological materials in that it is incompressible. Thus, Poisson's ratio, ν, is 0.5.

3.0 SURGICAL PROCEDURE

3.1 DEVELOPMENT OF RADIAL KERATOTOMY

The development of radial keratotomy began in Japan before contact lens technology was developed. In 1939, Dr. Sato of Japan experimented with making 35 posterior corneal incisions and 40 anterior incisions. At that time, the role of endothelium in corneal dehydration and clarity was unknown. Within six months to a year, Dr. Sato's patients developed corneal edema. An average of twenty years after the operations, there was an absence of endothelium and abnormal collageneous material posterior to Descemet's membrane.[47]

In 1972, Dr. Svyatoslav N. Fyodorov treated Boris Petrov, a sixteen year old Russian boy, whose glasses shattered in a fist fight lacerating his cornea. Once the glass was removed, Dr. Fyodorov observed that the boy's myopia decreased. He then reviewed the literature and modified Dr. Sato's technique by making only anterior incisions. Fyodorov and Durnev found that 16 incisions gave almost the same results as 20, 24, or 32, and are also credited with realizing varying the diameter of the optical zone altered the degree of correction. They determined the correction was a function of corneal diameter, optical zone diameter, radius of curvature, scleral rigidity, and a practical coefficient for

the surgeon.[38] An equation was formulated to predict the correction, yet in view of a constant varying with each surgeon's experience, the equation has no basis from an engineer's point of view.

Experience with the procedure has reduced the number of incisions from sixteen to eight. Eight incisions produce more than 80% of the effect of sixteen incisions. They provide fewer scars and potentially less glare, fewer overcorrections, and the option of making additional incisions for an undercorrected case. Additionally, the cornea remains rigid during the procedure.[47]

3.2 CLINICAL MEASUREMENT AND EVALUATION

Radial keratotomy is a surgical procedure of which almost every aspect remains under debate. Over the last decade, the controversy comes from surgical techniques differing with each surgeon's experience. Furthermore, the data has mostly been taken from office records intended for patient management, not research. Two organizations, the National Radial Keratotomy Group and the Keratorefractive Society, have been undertaken studies intended for research.[47]

To study the effectiveness of the procedure, measurements of refraction, visual acuity, and corneal shape are taken before and after surgery, and during several follow-up examinations. Visual acuity is measured by

standardized charts, corneal curvature by keratometry, and corneal topography through photokeratoscopy. Ocular dominance is also determined to study the effect of performing surgery on one eye. The near point of accommodation is found to study the effect on the ability to read without glasses. To quantify the complications after surgery, glare, endothelial cell size, the smallest diameter of the central zone, and the scar length and depth are measured.[47]

3.3 SUMMARY OF OPERATIVE PROCEDURE

On an outpatient basis, the surgery is performed under sterile conditions using an operating microscope. No mydraitic drops which cause pupil dilation are used. A small pupil helps to prevent accidental misplacement of the visual axis and reduces photophobia, sensitivity to light. A topical anesthia is applied, and the cornea is kept moist with a balanced salt solution.[47]

The visual axis is determined by asking the patient to fix upon a point within the microscope. The surgeon marks the epithelium with a hyperdermic needle. A dull marking trephine, a circular saw, is placed so that the intersection of the cross hairs within the trephine coincides with the small epithelial defect marking the visual axis. Setting the diameter of the trephine to the optical zone previously determined by the degree of myopia, the trephine makes a circular

indentation in the epithelium without damaging Bowman's membrane.[47]

The thickness is measured with an ultrasonic pachymeter at the center and at 90°, 180°, 270°, and 360° postions on the trephine mark. Using a screw type micrometer, the knife length is then advanced to 85% of the thinnest pachymeter reading. The diamond blade knife with a 45° cutting angle extends between two parallel footplates. The 1.27 mm wide, smooth flat surfaces of the footplate are designed to slide easily over the surface. Fixating the cornea at the limbus with forceps, the surgeon places the blade 180° away from the fixation point. The blade pierces the tissue directly without the footplate compressing or displacing the cornea, and then is moved slowly and smoothly to the limbus. The surgeon makes eight radial cuts equidistant around the cornea.[47] (Refer to figure 1 noting the order of the incisions.)

Each wound is irrigated with a balanced salt solution, and the depth of the incisions is verified with a micrometer. Antibotic drops are used post-operatively with the application of a mild pressure patch.[47]

3.4 COMPLICATIONS AND RESULTS

Severe complications such as perforation of the lens, microbial inflammation of the cornea, or inflammation of the internal structures of the eye are possible but highly unlikely to occur.[47]

After the incisions weaken the cornea, the intraocular pressure pushes the cornea into its new configuration and holds the deformed state until the wounds heal. Since the intraocular pressure varies during the day, patients experience fluctuating vision for 2-4 months until the cornea stabilizes. Sensitivity to light, photophobia, and glare are also noticed a few weeks after surgery. The wounds scatter light that may degrade the retinal image by decreasing contrast, but as the wounds heal, the scars become less opaque decreasing the glare and photophobia.[47] Each patient has different healing capacities which may result in only partial improvement of these symptoms and return of some myopia.

Villasenor, et al [45] observed that during surgery, a significant reduction in corneal thickness occured probably resulting from the heat of the operating room lights. Using ultrasonic pachymetry both centrally and peripherally, the decrease in thickness averaged 10% with a range of 7.8-15% with a modest reversal post-operatively. Surgeons may be cutting under the assumption the cornea thickens through edema. Thus the probability of perforation increases. Kramer [26] noted in at least 10% of the cases that perforation of the cornea occured thus damaging the endothelium.

Even if perforation does not occur, trephination and scalpel pressure may destroy and stretch the endothelial cells by indirectly stretching

the endothelial sheet. In addition, the posterior surface area is increased with deformation flattening the cells centrally and peripherally.[32] Miller and Weiss [32] observed membrane wrinkling and cell destruction for up to two cell widths on each side of the incision. The buckling of Descemet's membrane appeared to be proportional to the deformation produced. Along these same lines, Yamaguchi, et al [51] found the appearance of a fold in Descemet's membrane within a week after surgery. No mention was made as to how long the fold remained, but one ridge appeared underneath each incision and seemed to be under mechanical pressure. With these factors in mind, Miller and Weiss estimated a 10-20% cell loss whereas Hoffer, et al [19] concluded a mean endothelial loss of 10%. With a loss of this magnitude, the endothelial cells may be separated and will lead to edema. Considering the additional loss through aging, decades of follow-up may be necessary to determine if the loss is clinicially significant.

A wide range of discrepancy exists concerning the change in thickness following surgery. Bores [2] found that edema extended from the bottom of the incisions anteriorly, and in no case involved the central optical zone. In all of his cases, edema disappeared within five weeks. Reddy [36] also observed a return to the original pre-operative thickness. Schachar [38] stated that the thickness did not return to its previous depth; however, the edematous condition disappeared within 3-6 months. Furthermore, Fyodorov [40] concluded that the cornea became thicker by

40 μ at one year after surgery.

3.5 LITERATURE REVIEW

In the literature, the papers analyzing the cornea as a thin shell have been mostly limited to the cornea's response under the loading of an applanation tonometer. Providing a method for diagnosing glaucoma, a tonometer applies a small flat disk to the anterior surface estimating the intraocular pressure by the cornea's resistance to deformation. The first attempts used simple membrane theory to understand the tissue response to the compressive loading, yet a more rigorous model was necessary to improve the precision of the measurements. Schwartz [40] used a thin spherical, shallow shell to approximate the cornea, but as shown in the next section, the assumption of shallowness is not valid for the corneal geometric constraints. With regard to the differing elastic properties of each layer, Mow [32] predicted the deformation through thin shell theory. However, Kobayashi, et al. [24] pointed out that Nyquist's experimental data determined the material properties across the entire thickness of the cornea and not each layer. Later, Kobayashi and Woo [24], [48] modeled the elastic structural response by finite element analysis. They assumed Poisson's ratio to be 0.49, nearly incompressible, and incorporated the non-spherical geometry and non-homogeneous material properties of the corneo-scleral shell into their analysis. These studies have a limited application to the

conditions of this problem except for gaining insight into the material behavior.

Schachar, Black, and Huang [38] is the only paper in which a mathematical model for radial keratotomy is constructed. Considering the cornea as a thin spherical shell, they developed a linear small displacement model based on the principle of minimum total strain energy. The model was approximated analytically by the Rayleigh-Ritz method. In the formulation of the model, the bending component of strain was neglected, and the shell was assumed to be axi-symmetric, homogeneous, linearly elastic with $E = 4.86 \times 10^7$ dynes/cm^2, incompressible with $\nu = 0.45$, and orthotropic. Schachar, et al. stated that after the operation, the thickness was no longer equal to the pre-operative thickness. To consider the effective thickness, they kept the thickness constant, and modified Young's modulus as a function of meridional and circumferential arc length, the ratio of the incision depth to the thickness, and a coefficient representing the probability of cutting collagen fibrils. In this way, the orthotropic assumption was made, and they predicted the corneal deformation that would occur in a shell of uniform thickness as Young's modulus was decreased. They found that the normal movement near the optical zone to be about 50-75 μ forward. The entire cornea moved outward with most of the movement occurring near the optical zone. The small displacement produces large changes in curvature resulting in the flattening of the cornea with the

greatest amount in the central region. Schachar, et al. concluded that radial keratotomy deformed the cornea through stretching the entire cornea not through peripheral bulging as Fyodorov surmised.

4.0 PROBLEM DEFINITION

4.1 INTRODUCTION

The cornea is a thin shell loaded only by internal pressure. Intraocular pressure is applied uniformly to the posterior surface of the cornea, and therefore, is symmetric with respect to the entire shell. The following assumptions on the shell are made: axi-symmetric, spherical, homogeneous, isotropic, incompressible, and linearly elastic. The behavior of a spherical shell, whose thickness is a function of meridional arc length but whose elastic properties are independent of position, is analyzed.

The first section defines the geometric parameters of the problem and the parameters classifying the thin shell assumption. The following section formulates the governing equations of shell behavior under internal pressure loading, and the last section specifies the boundary conditions as a simply-supported shell.

4.2 GEOMETRY

Figure 6 illustrates the basic notation used to characterize a spherical shell. The cornea can be described as a thin shell bounded by its anterior and posterior surfaces. These two closely spaced curves do not have concentric radii of curvature; nevertheless, the behavior of the cornea is assumed to be governed by the behavior of the middle surface. In other words, the displacements throughout the shell can be determined by the displacement of the middle surface. As the middle surface's radius of curvature is defined as the average radius of the bounding surfaces, the middle surface is located equidistant from the anterior and posterior surfaces. The thickness of the shell can be specified along a normal to that surface at any given point as the distance between the anterior and posterior surfaces. Designating the form of the middle surface and the thickness at every point, the shell is defined geometrically.

The shell is generated by the rotation of a plane curve about a vertical axis. One principle line of curvature, the plane curve or the middle surface, is refered to as the meridian. The second line of curvature is defined by the rotation of any given point on the meridian about the vertical axis, forming a horizontal circle called the hoop. The positive directions are shown in Figure 7. In a shell of revolution, all geometric parameters are considered axisymmetric. Also, since the

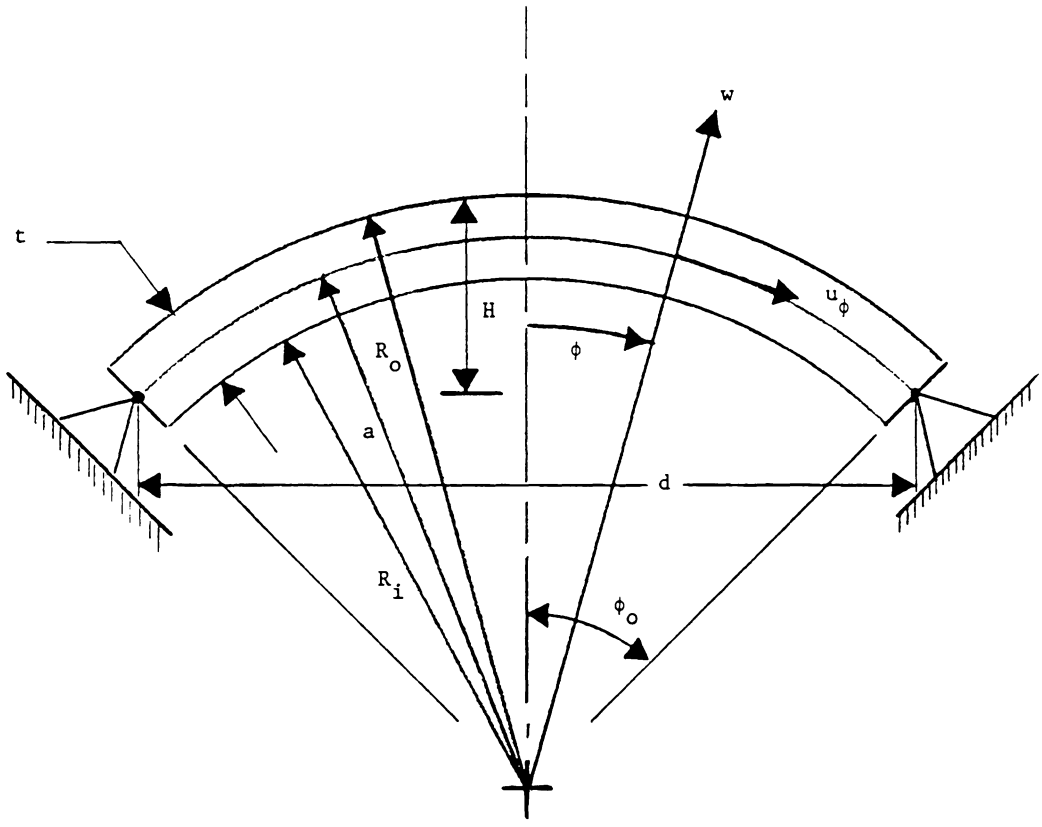

Figure 6. Cross-Sectional Geometry

loading of internal pressure on the cornea is symmetric, all shell spatial dependence to one independent variable, ϕ.

The cornea has the following dimensions:

$a = 7.2$ mm

$R_o = 7.8$ mm

$R_i = 6.6$ mm

$t_o = 0.5$ mm

$t_L = 0.66$ mm

$H = 2.684$ mm

$d = 11.7$ mm

$\phi_L = 48.5°$,

where:

$a \equiv$ radius of curvature of the middle surface

$R_o \equiv$ radius of curvature of the anterior surface

$R_i \equiv$ radius of curvature of the posterior surface

$t_o \equiv$ thickness at the corneal apex

$t_L \equiv$ thickness at the limbus

$H \equiv$ shell height

$d \equiv$ diameter of the base

$\phi_L \equiv$ angle of opening.

The plane through the outer visible border at which the limbus begins is the base of the cornea. The height of the shell is measured from the base to the anterior surface.

Two parameters are defined as criteria to satisfy the assumptions characterizing the shell type. The assumption of thinness requires that the thickness of the shell be small in comparision with the radius of curvature and the dimensions of the middle surface. For this to be valid, the ratio of thickness to radius of curvature is usually less than one-tenth. The requirement of shallowness is that the ratio of height to base diameter must be less than one-eighth. For the corneal dimensions,

$$\frac{t_o}{R} \sim \frac{0.5}{7.2} = 0.069$$

$$\frac{H}{d} \sim \frac{2.684}{11.7} = 0.229.$$

From these parameters, the cornea can be classified as a thin shell but cannot be further assumed to be a shallow one. The shell's thickness still is not thin enough to neglect the bending effects.

4.3 EQUATION FORMULATION

The technical theory of thin shells is based on certain approximate assumptions. The first of which, thinness, was discussed in the previous section. The other postulates are as follows:

- The displacements and displacement gradients are small in comparison with the thickness of the shell.
- The transverse normal stress is negligible in comparison to the in-plane normal stresses.
- Straight lines normal to the middle surface remain normal subsequent to deformation and undergo no change in length.

These simplifying assumptions allow a reasonable description of thin shell behavior in the development of general bending theory.

Figure 7 illustrates the resultant forces and moments acting on the shell element. The equations of static equilibrium for a spherical shell can be written as:

$$(N_\phi a\sin\phi)' - N_\theta a\cos\phi + Q_\phi a\sin\phi = 0 \tag{4.1}$$

$$(Q_\phi a\sin\phi)' - (N_\phi + N_\theta)a\sin\phi = pa^2\sin\phi \tag{4.2}$$

$$(M_\phi a\sin\phi)' - M_\theta a\cos\phi - Q_\phi a^2\sin\phi = 0, \tag{4.3}$$

where prime denotes a derivative with respect to ϕ, and the

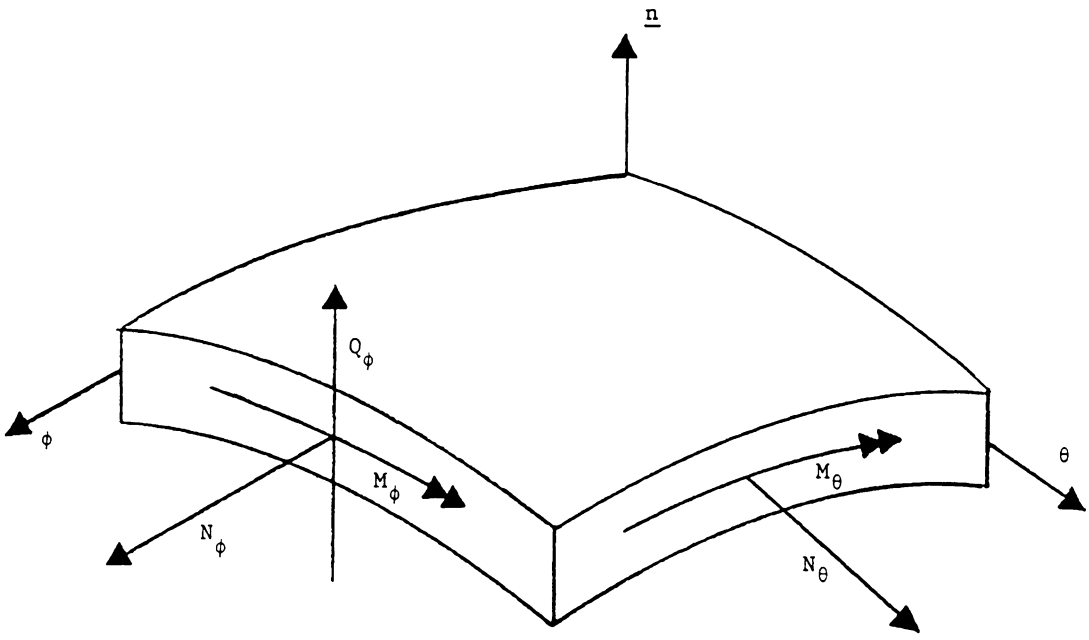

Figure 7. Resultant Forces and Moments Acting on a Spherical Element

resultant quanities are defined as:

$N \equiv$ resultant normal force

$M \equiv$ resultant moment

$Q \equiv$ resultant transverse shear force

$p \equiv$ internal pressure loaded perpendicular to the middle surface.

In order to consider variable thickness, the thickness is assumed to be a function of ϕ. Thus the flexural rigidity, D, and the extensional rigidity, K, are also dependent upon arc length, and are defined as:

$$t = t(\phi) \tag{4.4}$$

$$D(\phi) = \frac{Et^3(\phi)}{12(1-\nu^2)} \tag{4.5}$$

$$K(\phi) = \frac{Et(\phi)}{1-\nu^2} . \tag{4.6}$$

The constitutive equations are given by:

$$N_\phi = K(\phi)[\varepsilon_\phi + \nu\varepsilon_\theta] . \tag{4.7}$$

$$N_\theta = K(\phi)[\varepsilon_\theta + \nu\varepsilon_\phi] \tag{4.8}$$

$$M_\phi = D(\phi)[\chi_\phi + \nu\chi_\theta] \tag{4.9}$$

$$M_\theta = D(\phi)[\chi_\theta + \nu\chi_\phi], \tag{4.10}$$

where:

ε ≡ normal strain

χ ≡ change in curvature during deformation

u_ϕ ≡ displacement along the meridian

β_ϕ ≡ meridional angle of rotation.

The deformation is related to the strains through:

$$\varepsilon_\phi = \frac{u_\phi'}{a} + w \tag{4.11}$$

$$\varepsilon_\theta = \frac{1}{a}(u_\phi \cot\phi + w) \tag{4.12}$$

$$K_\phi = \frac{1}{a}\beta_\phi' \tag{4.13}$$

$$K_\theta = \frac{\beta_\phi}{a}\cot\phi, \tag{4.14}$$

where:

$$\beta_\phi = \frac{1}{a}(u_\phi - w'). \tag{4.15}$$

Including the equations of equilibrium, the constitutive relations, the strain-displacement relations, and the definition of β_ϕ, we have twelve equations and twelve unknowns. These equations can be reduced to two

simultaneous second-order ordinary differential equations in terms of the rotation, β_ϕ, and transverse shear, Q_ϕ. The derivation of the governing equations for a thin shell of variable thickness is available in Kraus' thin shell theory text [26]. For this case, we have:

$$\beta_\phi'' + (\cot\phi + \frac{3t'}{t})\beta_\phi' - \beta_\phi\cot^2\phi - \nu(1 - \frac{3\cot\phi t'}{t})\beta_\phi = \frac{a^2 Q_\phi}{D} \tag{4.16}$$

$$Q_\phi'' + (\cot\phi - \frac{t'}{t})Q_\phi' - (\cot^2\phi - \nu(1 + \frac{\cot\phi t'}{t}))Q_\phi = - Et\beta_\phi + \tfrac{1}{2}(1-\nu)pa\frac{t'}{t}. \tag{4.17}$$

Once β_ϕ and Q_ϕ are known, the stress resultants, moments, and displacements are obtained from:

$$N_\phi = Q_\phi\cot\phi + \tfrac{1}{2}pa \tag{4.18}$$

$$N_\theta = Q_\phi' + \tfrac{1}{2}pa \tag{4.19}$$

$$M_\phi = \frac{D(\phi)}{a}[\beta_\phi' + \nu\cot\phi\beta_\phi] \tag{4.20}$$

$$M_\theta = \frac{D(\phi)}{a}[\beta_\phi\cot\phi + \nu\beta_\phi'] \tag{4.21}$$

$$u_\phi = \sin\phi\left[\int_0^\phi \frac{a(1+\nu)}{Et(\phi)}(N_\phi - N_\phi)\frac{1}{\sin\phi}\,d\phi + C_2\right] \tag{4.22}$$

$$w = \frac{a}{Et(\phi)}(N_\theta - \nu N_\phi) - u_\phi\cot\phi, \tag{4.23}$$

where C_2 is the constant of integration satisfying the boundary condition on axial displacement of a reference point on the shell. The integral for determining u_ϕ is fixed at the origin. C_2 must be specified to fix the reference point at the limbus. In the derivation of the expression for N_ϕ, the boundary condition representing the net axial component of any end loads applied to the shell is set to zero.

4.4 BOUNDARY CONDITIONS

At the apex of the cornea, the transverse shear and rotation vanish to insure no tendency for the adjoining edge to slide with respect to one another. In addition, these terms must be set to zero so that the varibles will be finite as the cotangent approaches infinity at this point. Thus,

$$Q_\phi = \beta_\phi = 0 \qquad \text{at } \phi = 0^\circ. \tag{4.24}$$

With an abrupt geometric change in the limbal region, the circular fibers provide a natural boundary condition functioning essentially as a reinforcing ring. These fibers introduce an inward radial thrust

balancing the tension in the cornea and sclera. The ring almost entirely prevents the outward motion of the boundary while allowing rotation of the corneal surface. Thus, a simply supported edge is prescribed at the limbus.

The following conditions must be satisfied to define a simply supported edge:

- The edge is simply supported allowing for rotation, but there can be no momemt at the edge,

$$M_\phi = 0.$$

- There can be no displacement at the shell edge,

$$u_\phi = w = 0.$$

Specifying the boundary condition in terms of Q_ϕ and β_ϕ involves the formulation of two first-order differential equations. For the first condition, the stress-strain equation for M_ϕ is set to zero. Thus,

$$\beta_\phi' + \nu\beta_\phi \cot\phi = 0 \qquad \text{at } \phi = 0^\circ. \tag{4.25}$$

For the remaining condition, u_ϕ and w are expressed as the horizontal displacement δ:

$$\delta = u_\phi \cos\phi + w \sin\phi \tag{4.26}$$

$$\delta = (u_\phi \cot\phi + w)\sin\phi. \tag{4.27}$$

Recalling the strain-displacement relation for the circumferential strain and the stress-strain equations for the normal stress,

$$\delta = \varepsilon_\theta a \sin\phi \tag{4.28}$$

$$\delta = \frac{a\sin\phi}{K(\phi)(1-\nu^2)} (N_\phi - \nu N_\theta). \tag{4.29}$$

Since there can be no horizontal displacement,

$$N_\phi - \nu N_\theta = 0. \tag{4.30}$$

Finally, the condition is given in terms of Q_ϕ through the equations of equilibrium used in obtaining the normal stresses:

$$Q_\phi' - \nu Q_\phi \cot\phi - \tfrac{1}{2}(1-\nu)pa = 0. \tag{4.31}$$

To summarize the boundary conditions,

$$Q_\phi = 0,\ \beta_\phi = 0 \qquad \text{at } \phi = 0^\circ \tag{4.24}$$

$$\beta_\phi' + \nu\beta_\phi\cot\phi = 0 \qquad \text{at } \phi = \phi_L \tag{4.25}$$

$$Q_\phi' - \nu Q_\phi \cot\phi - \tfrac{1}{2}(1 - \nu)pa = 0. \tag{4.31}$$

5.0 NUMERICAL SOLUTION

5.1 INTRODUCTION

Finite difference techniques are used to solve the governing equations (§4.3) and the accompanying boundary conditions (§4.4).

Defined in the next section, the forward difference analogs are substituted into the governing equations to yield the finite difference equations. These equations are given in the third section, and the application of the difference analogs to the boundary conditions is discussed in the fourth section. Finally, the last section deals with solving the system of finite difference equations.

5.2 FINITE DIFFERENCE ANALOGS

The independent variable, ϕ, varies from 0° to ϕ_L. This interval is divided into R increments of equal spacing, $\Delta\phi$. Varying from 1 to R, the index i is used to indicate position along the ϕ-axis.

The forward difference analogs cooresonding to the discretized forms of the first and second derivatives of a dependent variable with respect to ϕ are defined by:

$$U'' = \frac{1}{\Delta\phi}(U_{i+1} - 2U_i + U_{i-1}) \tag{5.1}$$

$$U' = \frac{1}{2\Delta\phi}(U_{i+1} - U_{i-1}). \tag{5.2}$$

These analogs are second-order correct with all higher-order terms truncated.

5.3 FINITE DIFFERENCE EQUATIONS

The finite difference equations are obtained by substituting the forward difference analogs into the governing equations. The resulting set of simultaneous equations are of the form:

$$C_i^1 Q_{\phi_{i+1}} + B_i^1 Q_{\phi_i} + B_i^2 \beta_{\phi_i} + A_i^1 Q_{\phi_{i-1}} = D_i^1 \tag{5.3a}$$

$$C_i^4 \beta_{\phi_{i+1}} + B_i^3 Q_{\phi_i} + B_i^4 \beta_{\phi_i} + A_i^4 \beta_{\phi_{i-1}} = 0, \tag{5.3b}$$

where:

$$A_i^1 = \frac{1}{\Delta\phi^2} - \frac{1}{2\Delta\phi}\left(\cot\phi_i - \frac{t_i'}{t_i}\right) \tag{5.3c}$$

$$A_i^4 = \frac{1}{\Delta\phi^2} - \frac{1}{2\Delta\phi}\left(\cot\phi_i - \frac{3t_i'}{t_i}\right) \tag{5.3d}$$

$$B_i^1 = -\frac{2}{\Delta\phi^2} - \cot^2\phi_i + \nu\left(1 + \frac{\cot\phi_i t_i'}{t_i}\right) \tag{5.3e}$$

$$B_i^2 = Et_i \tag{5.3f}$$

$$B_i^3 = -\frac{12a^2(1-n2)}{Et_i^3} \tag{5.3g}$$

$$B_i^4 = -\frac{2}{\Delta\phi^2} - \cot^2\phi_i - \nu\left(1 - \frac{3\cot\phi t_i'}{t_i}\right) \tag{5.3h}$$

$$C_i^1 = \frac{1}{\Delta\phi^2} + \frac{1}{2\Delta\phi}\left(\cot\phi_i - \frac{t_i'}{t_i}\right) \tag{5.3i}$$

$$C_i^4 = \frac{1}{\Delta\phi^2} + \frac{1}{2\Delta\phi}\left(\cot\phi_i - \frac{3t_i'}{t_i}\right) \tag{5.3j}$$

$$D_i^1 = \tfrac{1}{2}(1-\nu)pa\frac{t_i'}{t_i}. \tag{5.3k}$$

This procedure yields two finite difference equations written about each discretized point for a total of 2×R equations and 2×R unknowns.

5.4 APPLICATION OF THE BOUNDARY COUNDITIONS TO THE FINITE DIFFERENCE EQUATIONS

The first and R^{th} finite difference equations at each endpoint are different from those given above.

At the apex, the values for β_ϕ and Q_ϕ are prescribed and are therefore known. These values are applied to the first finite difference equations such that:

$$\text{When } i=0, \quad Q_\phi = 0, \ \beta_\phi = 0, \tag{5.4}$$

$$\text{When } i=1, \quad C_1^1 Q_{\phi_2} \ B_1^1 Q_{\phi_1} + B_1^2 \beta_{\phi_1} = D_1^1 \tag{5.5a}$$

$$C_1^4 \beta_{\phi_2} + B_1^3 Q_{\phi_1} + B_1^4 \beta_{\phi_1} = 0, \tag{5.5b}$$

where $A_1^1 = A_1^4 = 0$ and the remaining coefficients are given by the expressions in §5.3.

In order to impose the boundary conditions at the limbus, a fictitious point outside the region is used to specify the value of the first derivative at the boundary. The analog of the first derivative is applied to the boundary conditions. Written for the $R+1^{th}$ value, these two relations are:

$$\beta_{\phi_{R+1}} = \beta_{\phi_{R-1}} - 2\Delta\phi(\nu\cot\phi_R\beta_{\phi_R}) \tag{5.6a}$$

$$Q_{\phi_{R+1}} = Q_{\phi_{R-1}} + 2\Delta\phi(\nu\cot\phi_R Q_{\phi_R} - \tfrac{1}{2}(1-\nu)pa). \tag{5.6b}$$

The dependent variables at the ficitious point are eliminated through substitution of these relations into the finite difference equation about the R^{th} point. The R^{th} equation is of the same form of those given in §5.3 with the coefficients specified as follows:

$$A_R^1 = A_R^4 = \frac{2}{\Delta\phi^2} \tag{5.6c}$$

$$B_R^1 = -\frac{2}{\Delta\phi^2} + \frac{2\nu\cot\phi_R}{\Delta\phi} - (1-\nu)\cot^2\phi_R + \nu \tag{5.6d}$$

$$B_R^2 = Et_R \tag{5.6e}$$

$$B_R^3 = -\frac{12a^2(1-n2)}{Et_R^3} \tag{5.6f}$$

$$B_R^4 = -\frac{2}{\Delta\phi^2} - \frac{2\nu\cot\phi_R}{\Delta\phi} - (1+\nu)\cot^2\phi - \nu \tag{5.6g}$$

$$C_R^1 = C_R^4 = 0 \tag{5.6h}$$

$$D_R^1 = \tfrac{1}{2}(1-\nu)pa\left[\frac{2}{\Delta\phi} + \cot\phi\right]. \tag{5.6i}$$

In this manner, the correct analogs are obtained at the boundaries.

5.5 SOLUTION OF THE FINITE DIFFERENCE EQUATIONS

The finite difference equations constitute a system of equations cooresponding to each equally spaced base point from 1 to R. Since the two governing equations are linear, the set of simultaneous equations generated are linear, and are solved by the algorithm for the bi-tridiagonal matrix. Accordingly, the values for the dependent variable are calculated at each point.

Once the values for Q_ϕ and β_ϕ are approximated, the stress resultants, moments, and displacements are found through the equations in §4.3. For the equations involving the first derivative, the forward difference analog is applied. To compute u_ϕ, the trapezoidal rule is used to approximate the integral.

The computer program for solving the system of finite difference equations is given in Appendix A.

The numerical approximation is compared to an illustrative example given in Krauss' [27]. The problem is that of an isotropic, hemispherical cap of constant thickness with clamped ends and loaded by internal pressure. In Figure 8 the non-dimensionalized N_θ, M_ϕ, and M_θ are plotted as functions of meridional position and of the ratio of R/h equivalent to 10 and 100. These results are almost identical to Krauss' general

solution in terms of hypergeometric functions. The close comparison lends credibility to this formulation and numerical procedure.

Direct comparison with a thin shell of variable thickness was not possible as a literature search turned up only one other effort in this area which was a shell loaded under its own weight [42].

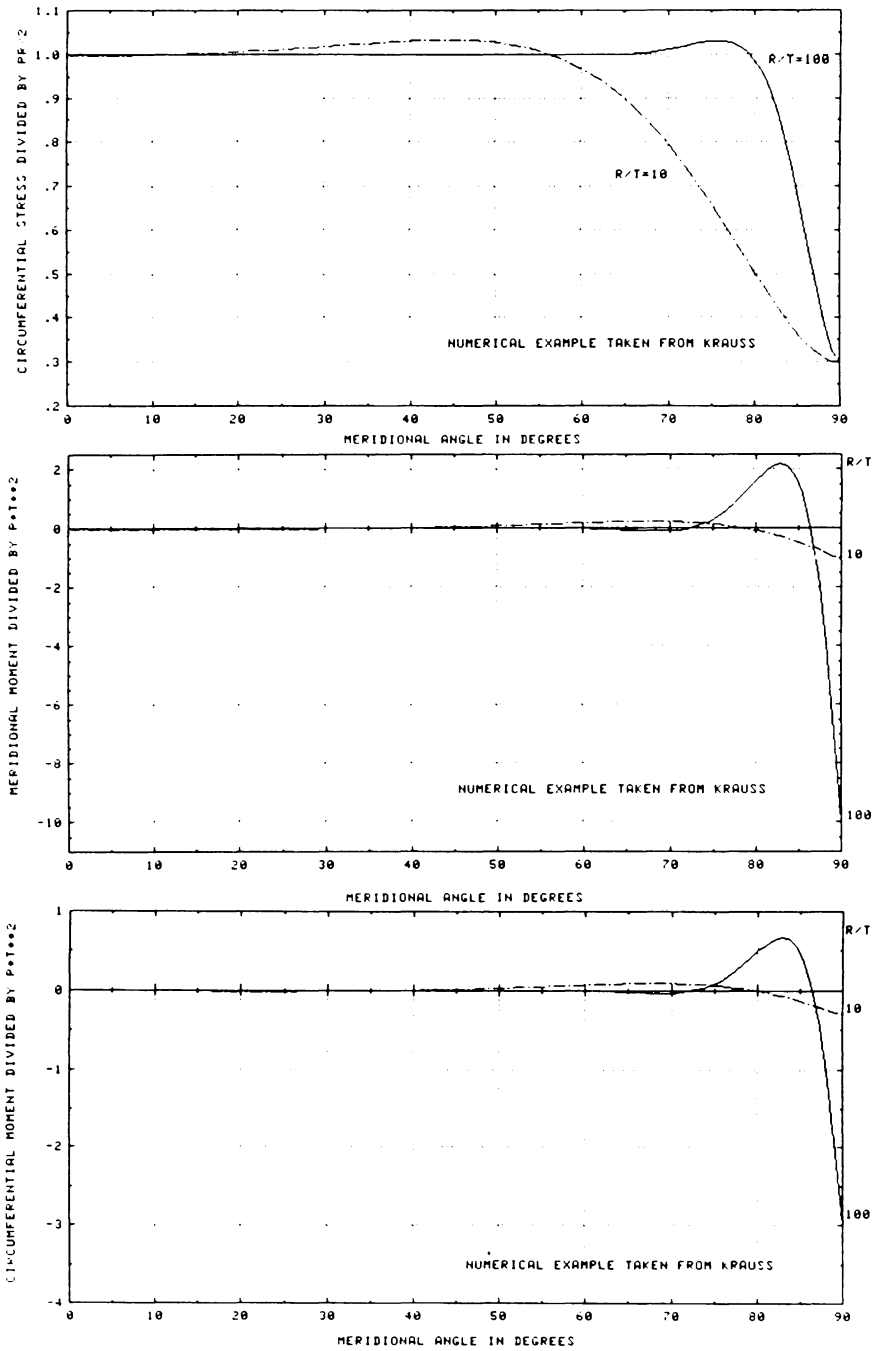

Figure 8. Circumferential Normal Force, Axial Moment, and Circumferential Moment Distributions for Kraus' Numerical Example: An isotropic, hemispherical shell of constant thickness with clamped ends and loaded by internal pressure.

6.0 RESULTS AND CONCLUSIONS

6.1 INTRODUCTION

The main objective of this investigation is to compare deformation fields in the cornea. First, a shell of constant curvature will be compared to a shell of natural curvature. Second, a shell of natural thickness will be compared to a shell with a 10% increase in natural thickness.

To gain insight into the cornea's natural configuration, a comparison is made between the displacement field predicted by a constant thickness shell model and the one of normally varying thickness. In the past, most analysis of the cornea have been based on uniform thickness and neglected bending stresses in the shell. The cornea's variable thickness increases the shell's efficiency in distributing the bending stresses.

The increasing thickness in the periphery of the shell attempts to model the edematous state resulting from the incisions. It is thought that the increasing depth would play a significant role in the corneal deformation after radial keratotomy. However, the results show that the displacement due to an increasing thickness is not great enough to

produce the results expected from radial keratotomy. In addition, the radius of curvature changes in the opposite direction. The primary contribution is believed to be the incisions, themselves, as they relieve the residual stresses in the cornea.

In the next section, the results comparing a shell of constant thickness to one of naturally varying thickness will be discussed. Then, the third section will present the results from increasing the normal thickness and deal with its effect on the cornea.

6.2 COMPARISON OF A CONSTANT THICKNESS AND A NATURALLY VARYING THICKNESS SHELL

Due to its curvature, a shell is able to transmit surface loads through membrane stresses parallel to the tangential plane. In general, thin shells are thick enough to carry loads by compressive, tensile and shear stress, but thin enough not to develop appreciable bending stresses. As discussed in §4.2, this is not the case in the cornea. Its thickness is dictated by bending disturbances rather than by membrane stresses.

Bending is introduced by the support condition at the limbus. At the boundary, internal pressure tends to move the shell out while the reinforcing ring constrains the shell and tends to move it in. When the reactions are not tangent to the meridian along the boundary, bending

stresses occur in the neighborhood of the boundary. Hence, it is necessary to increase the thickness to increase the bending rigidity of the shell.

To model the normally varying thickness of the cornea, the following thickness function is assumed:

$$t(\phi) = t_o(1 + A(\sin\phi)),$$

where A is a coefficient determined by the thickness at the limbus, t_L.

Figures 9-10 are plots of the transverse shear, normal, and bending resultant force distributions for a shell of constant thickness and one of normally varying thickness. The difference in the transverse shear and normal distributions between the constant and the normal thickness cases is slight compared to the reduction in bending moments. Figure 10 shows that the moments are greater in the periphery of the shell, and the natural thickness of the cornea is very efficient in transmitting the bending stresses introduced at the boundaries.

Figure 11 is a plot of the displacements in the cornea, and plots those displacements as the deformed shape of the middle surface. At the apex, the cornea is displaced about 1 μ as the thickness is changed from

constant to normal. The shell of greater thickness does not deform as much when loaded by internal pressure. This could be predicted by the increased bending rigidity of the shell.

Figure 12 is a plot of the change in curvature and angle of rotation of the middle surface during deformation. As can be seen in both plots, the change in curvature in the periphery decreases as the shell depth increases from constant to normal. Recalling κ_ϕ is the inverse of the change in radius of curvature, the decrease in κ_ϕ increases the radius of curvature in this region. Whereas at the central cornea, the increase in κ_ϕ decreases the radius of curvature. Figure 11 of the deformed middle surface better illustrates the difference in curvature. Under normal thickness, the cornea flattens in the periphery and steepens toward the center much like its normal shape. The cornea owes a portion of its curvature to the variable thickness of the shell.

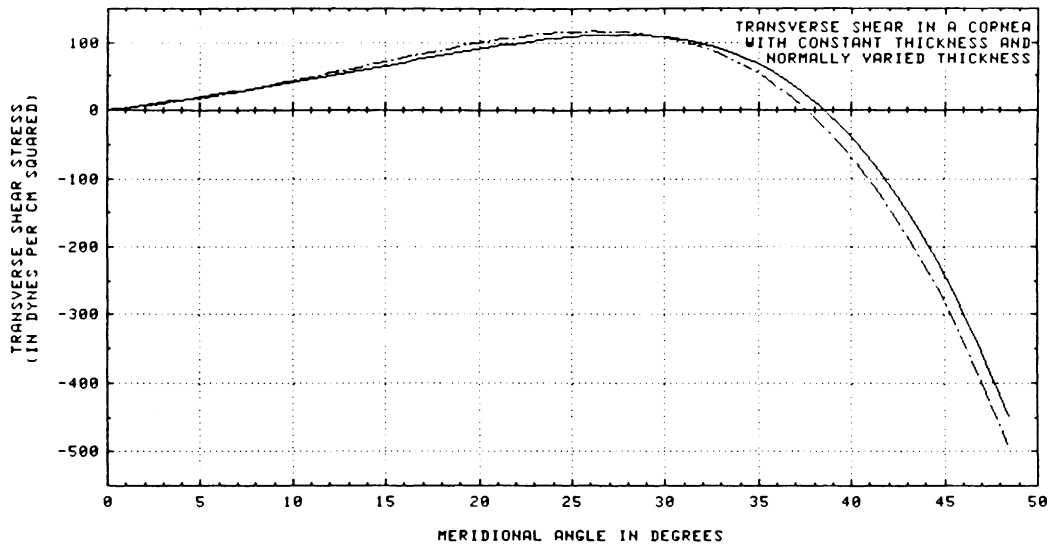

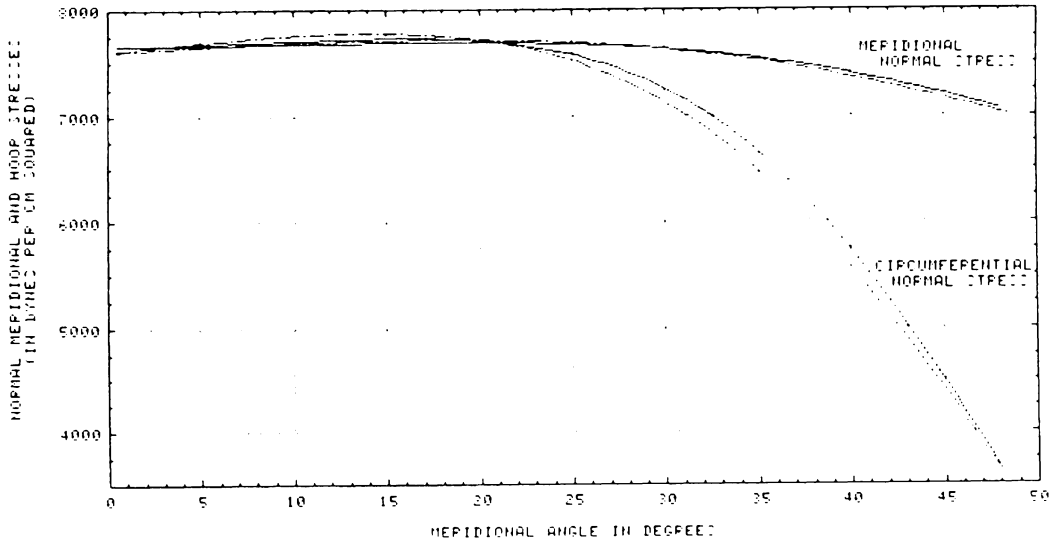

Figure 9. Resultant Transverse Shear and Normal Force Distributions for a Cornea of Constant Thickness and of Normal Thickness: The solid line represents the cornea of constant thickness while the dot dash line represent one of normally varied thickness.

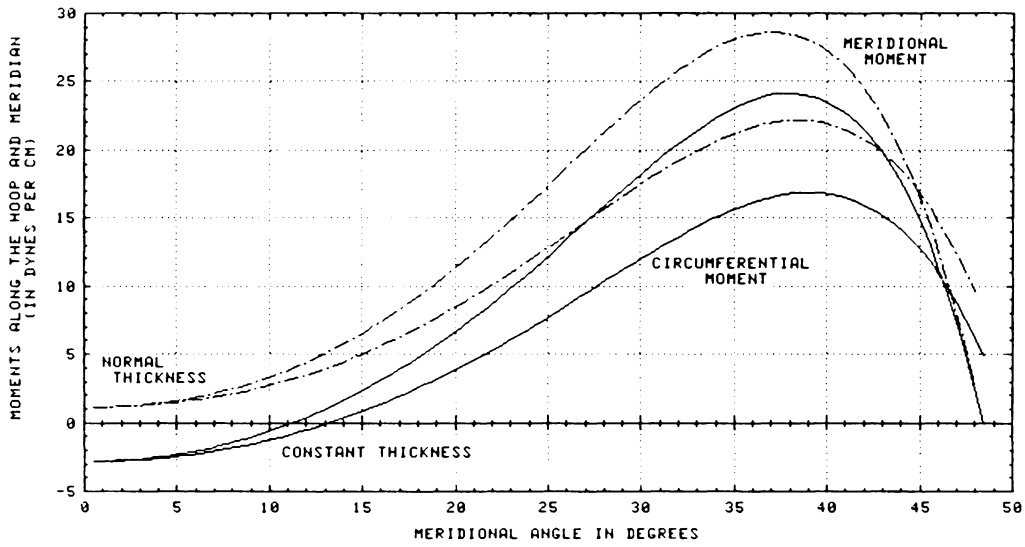

Figure 10. Resultant Bending Force Distributions for a Cornea of Constant Thickness and of Normal Thickness

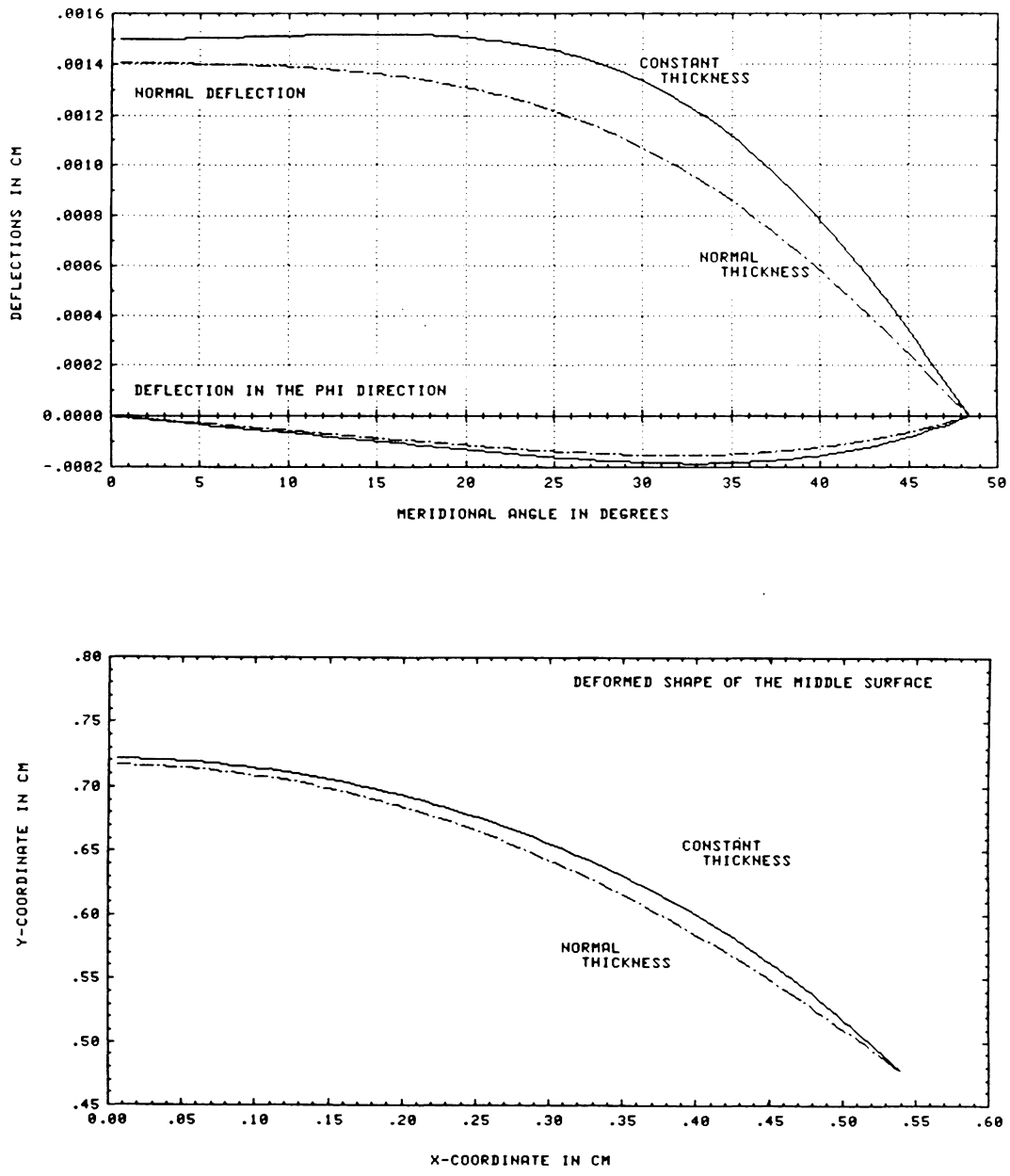

Figure 11. Displacements and Deformed Shape of the Middle Surface in a Cornea of Constant Thickness and of Normal Thickness

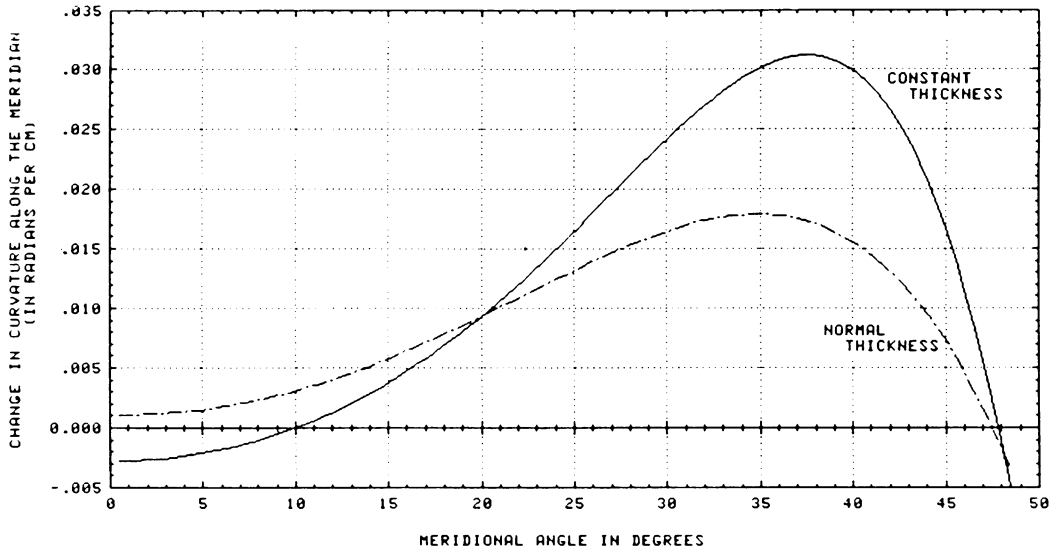

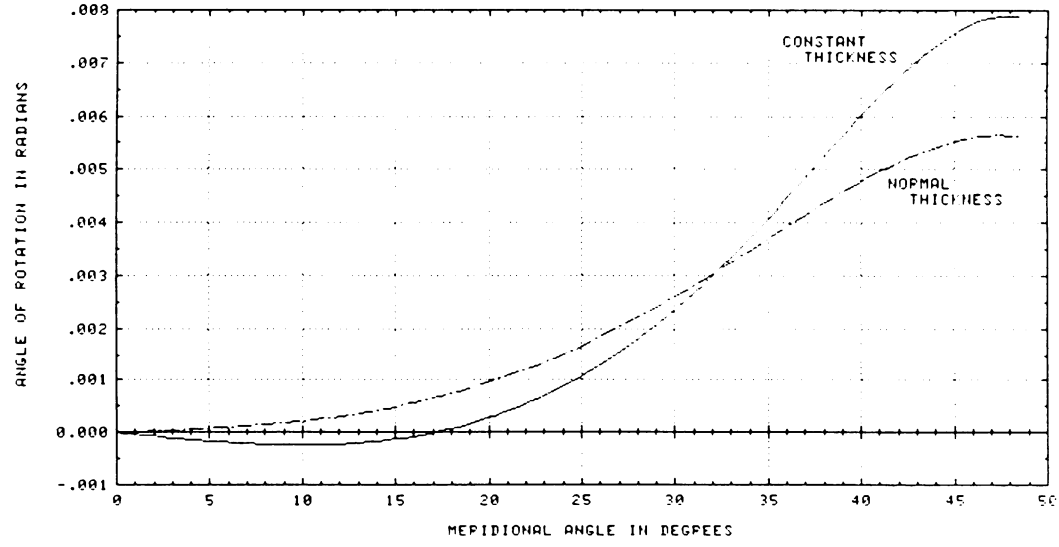

Figure 12. Change in Curvature and Angle of Rotation for a Cornea of Constant Thickness and of Normal Thickness

6.3 RESULTS FROM INCREASING THE NATURAL THICKNESS OF THE CORNEA

The natural corneal thickness is increased by 10% in the peripheral cornea, and the transition to the central optical zone is fit with a sine curve. Figure 13 illustrates the thickness function itself and the effective shape of the anterior surface.

The distribution of shell variables across the shell are plotted in Figures 14-17. The jump in the thickness curve at 10° results from the sharp transition in the effective thickness. Intuitively, one would expect the results of an additional increase in thickness to be similiar to the results of the previous section, except not as dramatic. This is indeed the case.

With an increase in thickness, the normal displacement is less than 0.3 μ at the apex of the cornea while the difference in radius of curvature is on the order of 5 μ. Referring to Table 1, the change in refractive power of the cornea is minute in comparison to the change needed to correct myopia.

The deformed shape of the middle surface is graphed in Figure 17. With the increased bending rigidity of the periphery, the cornea moves inward becoming flatter in the peripheral zone and steeper in the central zone.

This movement is exactly opposite of that experienced by radial keratotomy.

Physically, the movement of the cornea with increased thickness is limited by the virtue of the lateral support in a shell structure. The meridians of the shell are supported by the parallels which restrain their lateral displacement by developing circumferential stresses. The hoop stresses permit a small amount of movement in and out of the meridian but do not allow large displacement. Consequently, incisions must be made along the meridians to release the hoop stresses, and allow large displacements exhibited by radial keratotomy.

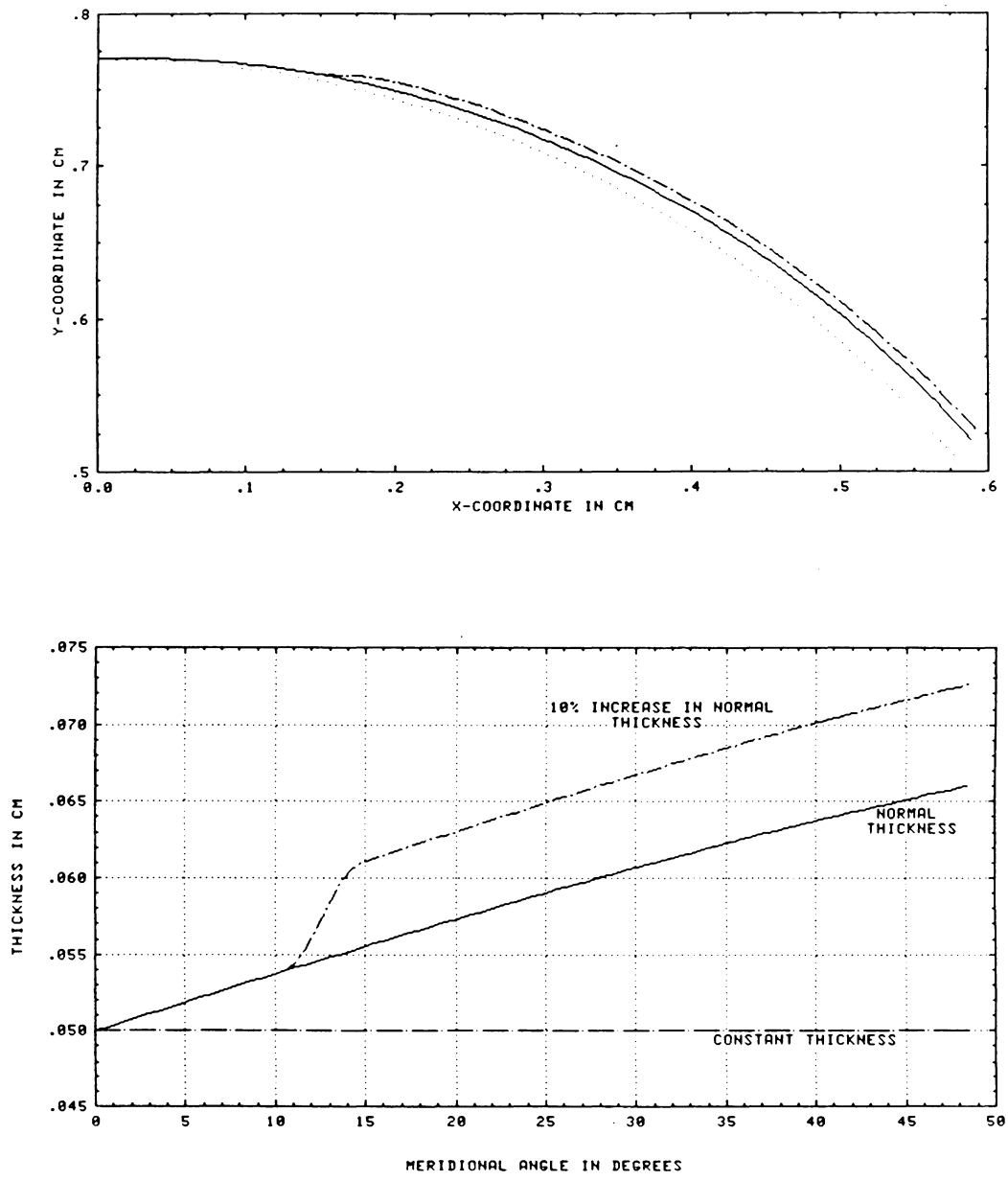

Figure 13. Effective Shape of the Anterior Surface and Thickness Function for a Constant, Normal, and 10% Increased Normal Thickness: In the first graph, the point dots represent the cornea of constant thickness; the solid line represents normal thickness; and the dot dash line represents a 10% increase in normal thickness.

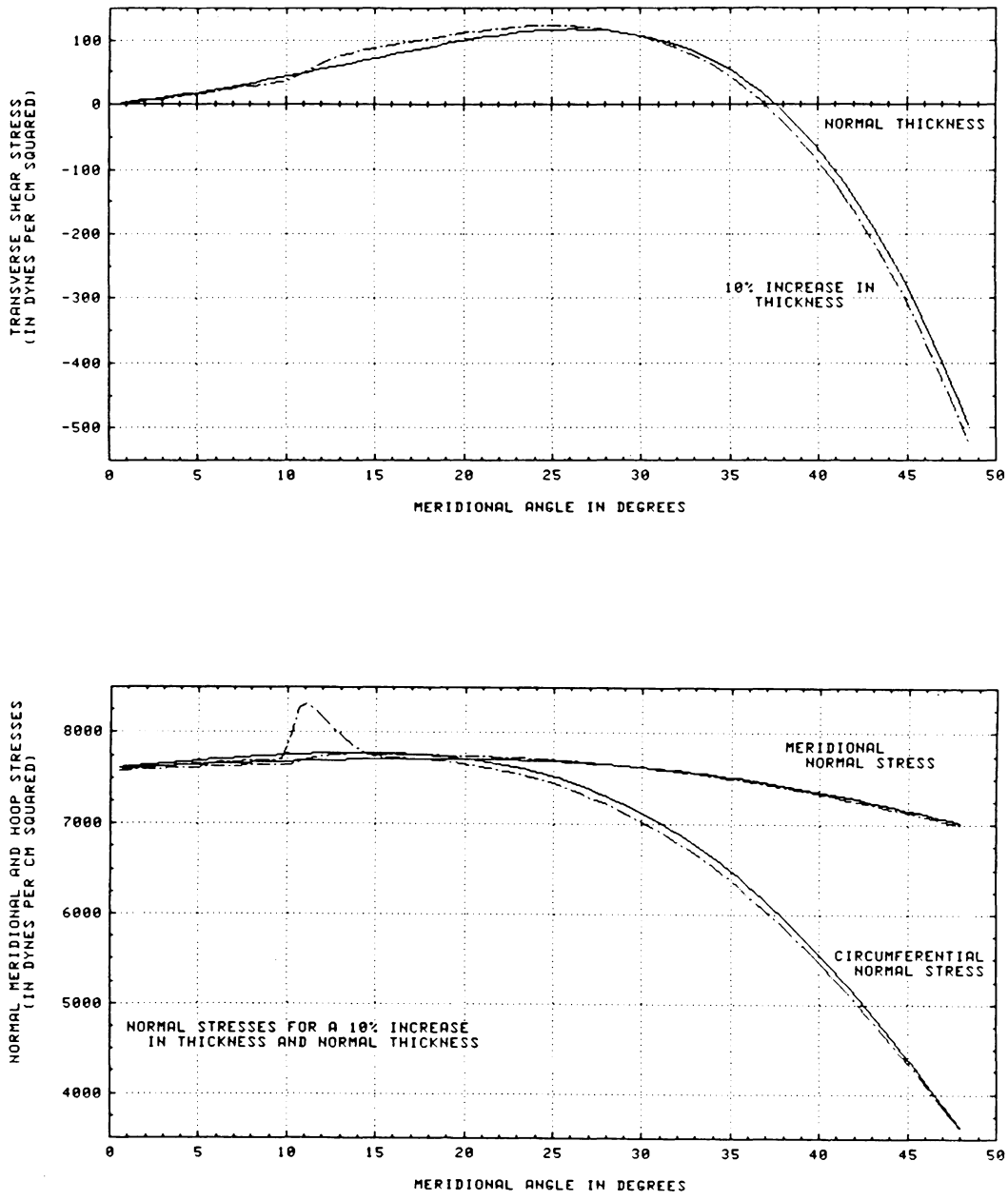

Figure 14. Resultant Transverse Shear and Normal Force Distribution for a Cornea of Normal Thickness and of a 10% Increase in Normal Thickness: The solid line represents the cornea of normal thickness while the dot dash line represents one with a 10% increase in normal thickness.

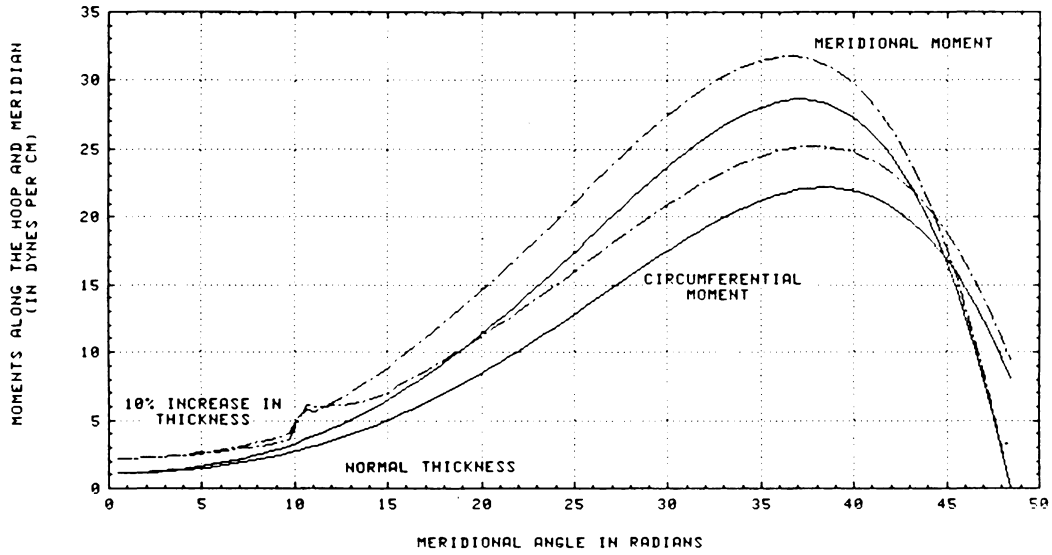

Figure 15. Resulant Bending Force Distributions for a Cornea of Normal Thickness and of a 10% Increase in Normal Thickness

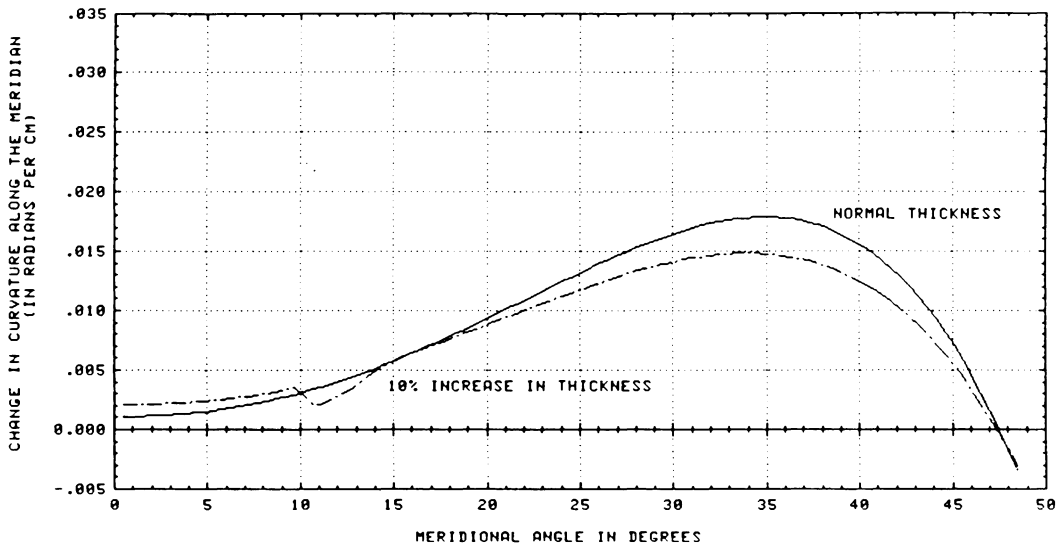

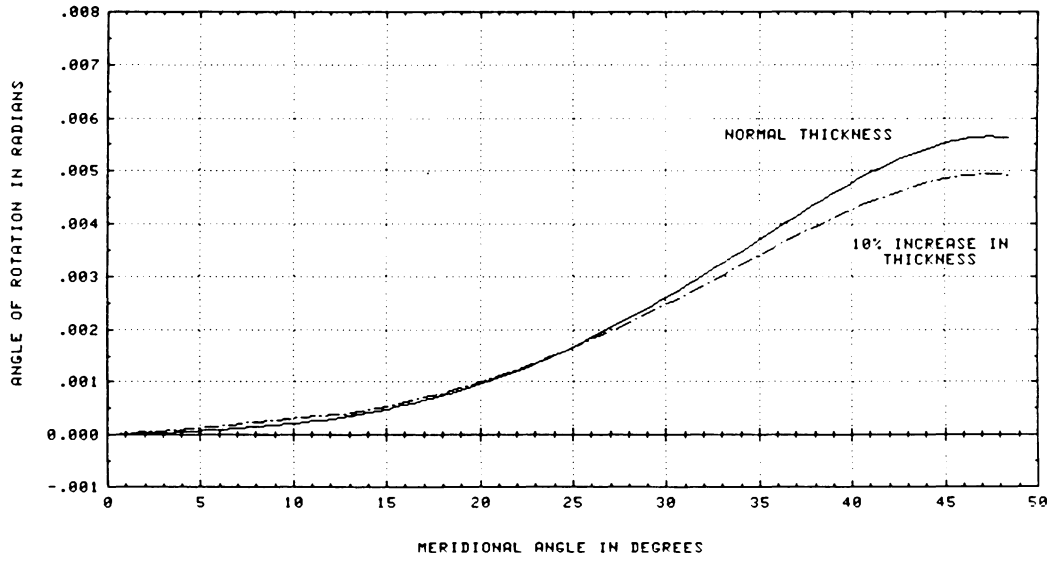

Figure 16. Change in Curvature and Angle of Rotation for a Cornea of Normal Thickness and of a 10% Increase in Normal Thickness

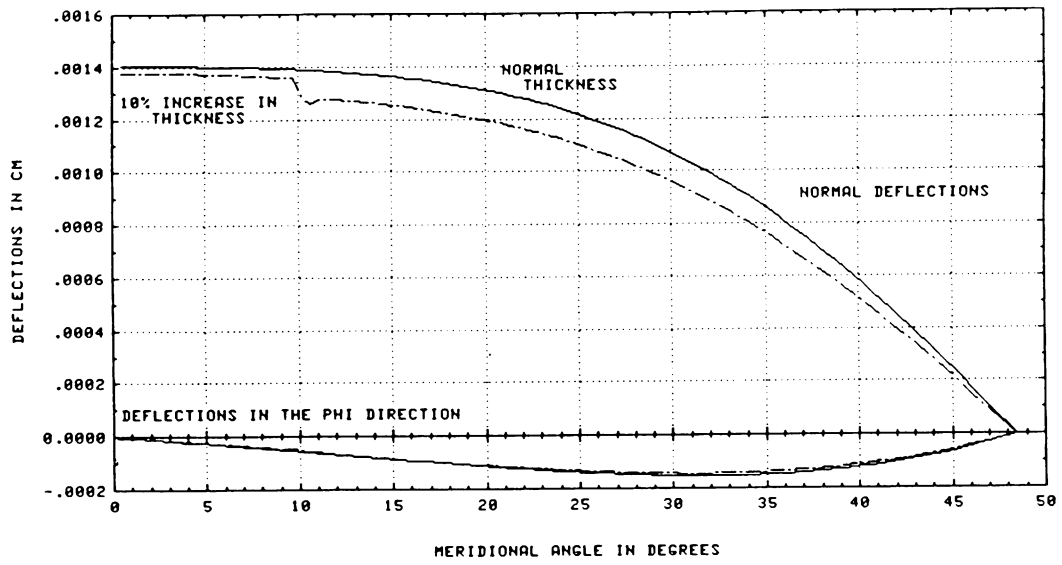

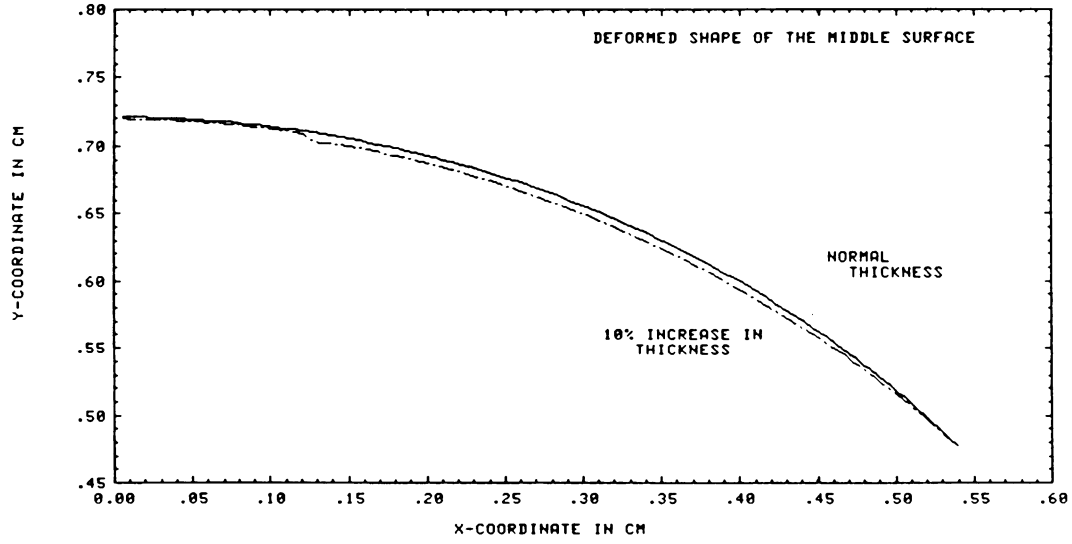

Figure 17. Displacements and Deformed Shape of the Middle Surface in a Cornea of Normal Thickness and of a 10% Increase in Normal Thickness

Table 1. Comparison of Refractive Parameters•

	Normal Deflection w (μ)	Change In Curvature (10^2)	Deformed Radius of Curvature (mm)	Dioptic Power D
Constant Thickness	15.0	-2.785	7.215	46.78
Normal Thickness	14.0	1.096	7.194	46.91
10% Increase in Thickness	13.8	2.140	7.189	46.95

• The refractive power of the cornea, D, is calculated by the standard keratometry equation with the index of refraction, n, assumed to be 1.3375. The data can be compared to a normal cornea with a radius of 7.2 mm where D = 46.88.

6.4 CONCLUSIONS

This thesis accomplishes the following:

1. The cornea is defined as a thin shell of variable thickness, and modeled by the general shell equations of elasticity.

2. This formulation is the first appearance of an analysis of a cornea of variable thickness taking into consideration the contribution of bending stress.

3. The governing equations for a normal cornea under the loading of intraocular pressure are solved through finite difference techniques.

4. In the comparison of a cornea of constant thickness and one of normal thickness, it is concluded that the normal curvature of the cornea is influenced by its variable thickness. The bending rigidity of the cornea is increased with increasing thickness.

5. The increase in thickness in the edematous state resulting from radial keratotomy is modeled by a 10% increase in the normal thickness in the area of the incisions. Results indicate a further stiffening of the cornea and more importantly an increase in

curvature at the apex. This is opposite to the desired decrease in curvature for radial keratotomy. Corneal displacement is minute in comparison to the displacement needed to correct myopia. Thus, edema induced by other techniques in the hope of reversing myopia could not produce the desired results.

6. In order to model radial keratotomy, the model must take into account the circumferential weakening produced by the incisions and the subsequent healing in the deformed state.

To model the incisions, future efforts could consider the orthotropic properties of the cornea as functions of position such that $E_\phi = E_\phi(\phi,\theta)$ and $E_\theta = E_\theta(\phi,\theta)$. By varying Young's modulus along the meridian, the length of incisions could be modeled. With Young's modulus varying periodically along the circumference, the discontinuity in hoop stresses caused by the incision could be taken into account. Another approach might be to relax the spherical assumption and introduce r_θ as a function of arc length. The incision opening necessary to deform the cornea to a desired state could be determined by altering the circumferential radius in the incised area.

A.0 COMPUTER CODE FOR FINITE DIFFERENCE SOLUTION

```
C  THIS PROGRAM WILL SOLVE THE THIN SHELL EQUATIONS FOR A SPHERICAL
C    SHELL OF VARIABLE THICKNESS UNDERINTERNAL PRESSURE ONLY
C    USING FINITE DIFFERENCE TECHNIQUES.
C
C
      REAL*8 EL1(101), EL2(101), EL3(101),EL4(101),B2(101),B3(101),
     1  G1(101), G2(101), B1(101), A1(101), B4(101), C1(101), D1(101),
     2  T1(101), X(101), CT(101), T2(101), T3(101), T4(101),T5(101),
     3  QPHI(101), B(101), T(101), DT(101), DDT(101), BT1(101),T7(101),
     4  BT2(101), BT3(101), BT4(101), DT1(101), DT2(101), NPHI(101),
     5  NHOOP(101), MPHI(101), MHOOP(101), KPHI(101), KHOOP(101),
     6  UPHI(101), W(101), BPHI(101), F(101), A4(101), C4(101),T8(101),
     7  R, PHI, DX, P, E, POIS, TF, A, T6, ANG, PI, DEG(101), C, CI,
     8  XI(101), YI(101), XF(101), YF(101), DEL, PR, D(101), DI, T9(101)
C
C  IN IS THE NUMBER OF INCREMENTS.
C  DX IS THE LENGTH OF THE INCREMENT.
C  PHI IS THE LENGTH FROM THE APEX TO THE LIMBUS IN RADIANS.
C  R IS THE RADIUS OF CURVATURE IN CM.
C
      IN=100
      PI=3.1415392654D00
      PHI=0.846D00
      R=0.72D00
      DX=PHI/IN
      X(1)=0.0D00
      T(1)=0.05D00
      DT(1)=0.0D00
      DDT(1)=0.0D00
      INM1=IN-1
      INP1=IN+1
C
C  P IS THE INTRAOCULAR PRESSURE IN DYNES PER CM SQUARED.
C  POIS IS POISSON'S RATIO.
C  E IS YOUNG'S MODULUS IN DYNES PER CM SQUARED.
C
      P=20666.7D00
      POIS=0.5D00
      E=48600000.0D00
C
C  FOR A CHANGE IN THICKNESS, SOLVE FOR THE COEFFICIENT A.
C
```

```
      DEL=0.05D00
      TF=0.066D00
      A=(TF/DEL-1.0D00)/DSIN(PHI)
C
C  FIND THE THICKNESS AT EACH POINT, WHERE T IS THE THICKNESS, DT
C    IS THE FIRST DERIVATIVE OF THE THICKNESS WITH RESPECT TO
C    PHI, AND DDT IS THE SECOND DERIVATIVE WITH RESPECT TO PHI.
C
C  CALCULATE T ACCORDING TO THE NORMAL THICKNESS FUNCTION.
C
      DO 4 I=2,INP1
      X(I)=X(I-1)+DX
      T(I)=DEL*(1.0D00+A*DSIN(X(I)))
      DT(I)=DEL*A*DCOS(X(I))
    4 DDT(I)=-DEL*A*DSIN(X(I))
C
C  INCREASE T BY 10% IN THE PERIPHERY.
C
      DO 5 I=32,INP1
    5 T(I)=T(I)*1.10D00
C
C  CALCULATE T ACROSS THE TRANSITION REGION.
C
      DI=T(32)-T(22)
C
      DO 6 I=22,32
      N=I-32
      ANG=PI*(1.0D00+N/10.D00)
    6 T(I)=T(22)+DI*(1.0D00+DCOS(ANG))/2.0D00
C
      DO 7 I=22,IN
      DT(I)=(T(I+1)-T(I-1))/(2.0D00*DX)
    7 DDT(I)=(T(I+1)-2.0D00*T(I)+T(I-1))/(DX**2)
C
C  XI, YI ARE THE COORDINATES OF THE MIDDLE SURFACE BEFORE DEFORMATION.
C
      DO 8 I=1,101
      XI(I)=R*DSIN(X(I))
      YI(I)=R*DCOS(X(I))
    8 CONTINUE
C
      DO 9 I=1,INP1
    9 DEG(I)=X(I)*180.0D00/PI

      WRITE(6,140) A,(DEG(I),T(I),XI(I),YI(I),I=1,101)
  140 FORMAT(//1X,'A = ',E14.7///101(4(5X,E14.7)/)///)
C
C  THEN WE WILL CALCULATE THE COMPONENTS OF THE COEFFICIENTS OF THE
```

```
C     FINITE DIFFERENCE EQUATIONS.
C
      DO 10 I=2,INP1
      CT(I)=1.0D00/DTAN(X(I))
      T1(I)=1.0D00/(DX**2)
      T2(I)=CT(I)**2
      T3(I)=DT(I)*CT(I)/T(I)
      T4(I)=(CT(I)-DT(I)/T(I))/(2.0D00*DX)
   10 T5(I)=(CT(I)+3.0D00*DT(I)/T(I))/(2.0D00*DX)
C
C  CALCULATE THE COEFFICIENTS OF THE FINITE DIFFERENCE EQUATIONS FROM
C     POINT 1 TO R-1
C
      DO 11 I=2,IN
      A1(I)=T1(I)-T4(I)
      A4(I)=T1(I)-T5(I)
      B1(I)=-2.0D00*T1(I)-T2(I)+POIS*(1.0D00+T3(I))
      B2(I)=E*T(I)
      B3(I)=-12.0D00*R**2*(1.0D00-POIS**2)/(E*T(I)**3)
      B4(I)=-2.0D00*T1(I)-T2(I)-POIS*(1.0D00-3.0D00*T3(I))
      C1(I)=T1(I)+T4(I)
      C4(I)=T1(I)+T5(I)
   11 D1(I)=POIS*P*R*DT(I)/(2.0D00*T(I))
C
C  INITIALIZE THE VALUES OF THE FUNCTIONS.
C
      DO 12 I=1,INP1
      QPHI(I)=0.0D00
   12 B(I)=0.0D00
C
C
C  FROM THE BOUNDARY CONDITIONS AT THE APEX, INITIALIZE THE COEFFICIENT
C     A FOR THE FINITE DIFFERENCE EQUATION AT POINT 3.
C
      A1(2)=0.0D00
      A4(2)=0.0D00
C
C  CALCULATE THE COEFFICIENTS OF THE RTH FINITE DIFFERENCE EQUATION
C     ACCORDING TO THE PRESCRIBED BOUNDARY CONDITIONS FOR U.
C
      T6=2.0D00*POIS*CT(INP1)/DX
C
      A1(INP1)=2.0D00*T1(INP1)
      A4(INP1)=A1(INP1)
      B1(INP1)=-2.0D00*T1(INP1)+T6-POIS*T2(INP1)+POIS
      B2(INP1)=E*T(INP1)
      B3(INP1)=-12.0D00*R**2*(1.0D00-POIS**2)/(E*T(INP1)**3)
      B4(INP1)=-2.0D00*T1(INP1)-T6-(1.0D00+POIS)*T2(INP1)-POIS
```

```
      D1(INP1)=POIS*P*R/2.0D00*(2.0D00/DX+CT(INP1))
      C1(INP1)=0.0D00
      C4(INP1)=0.0D00
C
C  INITIALIZE THE VALUES OF THE FUNCTIONS COMPUTED IN THE ALGORITHM
C    ACCORDING TO THE FIRST EQUATION AT POINT 1.
C
      BT1(2)=B1(2)
      BT2(2)=B2(2)
      BT3(2)=B3(2)
      BT4(2)=B4(2)
      DT1(2)=D1(2)
      DT2(2)=0.0D00
      EM=B1(2)*B4(2)-B2(2)*B3(2)
      EL1(2)=B4(2)*C1(2)/EM
      EL2(2)=-B2(2)*C4(2)/EM
      EL3(2)=-B3(2)*C1(2)/EM
      EL4(2)=B1(2)*C4(2)/EM
      G1(2)=B4(2)*D1(2)/EM
      G2(2)=-B3(2)*D1(2)/EM
C
C  COMPUTATION OF THE FUNCTIONS COMPUTED FOR THE BI-TRIDIAGONAL
C    MATRIX ALGORITHM.
C
      DO 13 I=3,INP1
C
      BT1(I)=B1(I)-A1(I)*EL1(I-1)
      BT2(I)=B2(I)-A1(I)*EL2(I-1)
      BT3(I)=B3(I)-A4(I)*EL3(I-1)
      BT4(I)=B4(I)-A4(I)*EL4(I-1)
C
      EM=BT1(I)*BT4(I)-BT2(I)*BT3(I)
C
      EL1(I)=BT4(I)*C1(I)/EM
      EL2(I)=-BT2(I)*C4(I)/EM
      EL3(I)=-BT3(I)*C1(I)/EM
      EL4(I)=BT1(I)*C4(I)/EM
C
      DT1(I)=D1(I)-A1(I)*G1(I-1)
      DT2(I)=-A4(I)*G2(I-1)
C
      G1(I)=(BT4(I)*DT1(I)-BT2(I)*DT2(I))/EM
   13 G2(I)=(BT1(I)*DT2(I)-BT3(I)*DT1(I))/EM
C
C
C
C  THE BACK SOLUTION IS:
C
```

```
      QPHI(INP1)=G1(INP1)
      B(INP1)=G2(INP1)
C
      DO 14 I=1,INM1
      J=INP1-I
      QPHI(J)=G1(J)-EL1(J)*QPHI(J+1)-EL2(J)*B(J+1)
   14 B(J)=G2(J)-EL3(J)*QPHI(J+1)-EL4(J)*B(J+1)
C
C  QPHI IS THE TRANSVERSE SHEAR FORCE IN THE PHI-DIRECTION.
C  B IS THE ANGLE OF ROTATION.
C
C
C  ONCE QPHI AND BETA ARE KNOWN AT EACH POINT, WE CAN THEN CALCULATE
C    THE NORMAL STRESSES, MOMENTS, AND CHANGES IN CURVATURE:
C    WHERE NQHI IS THE RESULTANT NORMAL FORCE IN THE QHI-DIRECTION,
C    NHOOP IS THE RESULTANT NORMAL FORCE IN THE THETA-DIRECTION,
C    MPHI IS THE MOMENT IN THE PHI-DIRECTION, MHOOP IS THE MOMENT IN
C    THE THETA-DIRECTION, KPHI IS THE CHANGE IN CURVATURE IN THE
C    PHI-DIRECTION, AND THE KHOOP IS THE CHANGE IN CURVATURE IN THE
C    THETA-DIRECTION.
C
      PR=P*R/2.0D00
C
      DO 15 I=2,INP1
   15 T8(I)=B(I)*CT(I)
C
      NPHI(1)=PR
      NHOOP(1)=PR
      KHOOP(1)=0.0D00
      KPHI(1)=0.0D00
      KPHI(INP1)=-POIS/R*T8(INP1)
      MPHI(1)=0.0D00
      MHOOP(1)=0.0D00
      MPHI(INP1)=0.0D00
      MHOOP(INP1)=E*T(INP1)**3*T8(INP1)/(12.0D00*R)
C
      DO 16 I=2,INP1
      NPHI(I)=QPHI(I)*CT(I)+PR
   16 KHOOP(I)=T8(I)/R
C
      NHOOP(INP1)=POIS*NPHI(INP1)
C
      DO 17 I=2,IN
      T7(I)=(B(I+1)-B(I-1))/(2.0D00*DX)
      D(I)=E*T(I)**3/(R*12.0D00*(1.0D00-POIS**2))
C
      NHOOP(I)=(QPHI(I+1)-QPHI(I-1))/(2.0D00*DX)+PR
      MPHI(I)=D(I)*(T7(I)+POIS*T8(I))
```

```
      MHOOP(I)=D(I)*(T8(I)+POIS*T7(I))
   17 KPHI(I)=T7(I)/R
C
C  NOW WE CAN ALSO CALCULATE THE DEFLECTIONS WHERE UPHI IS THE
C    DEFLECTION IN THE PHI-DIRECTION AND W IS THE DEFLECTION NORMAL TO
C    THE SURFACE.  THE TRAPEZOIDAL RULE IS USED TO EVALUATE THE INTEGRAL
C    IN THE EXPRESSION FOR UPHI.
C
      F(1)=0.0D00
      UPHI(1)=0.0D00
      UPHI(INP1)=0.0D00
      W(1)=R*NPHI(1)*POIS/(E*T(1))
      W(INP1)=0.0D00
      T9(1)=0.0D00
C
      DO 18 I=2,INP1
      F(I)=(NPHI(I)-NHOOP(I))/(T(I)*DSIN(X(I)))
   18 T9(I)=T9(I-1)+F(I-1)+F(I)
C
      CI=R*(1.0D00+POIS)/E
      C=-T9(INP1)*CI*DX/2.0D00
C
      DO 19 J=2,INP1
      UPHI(J)=DSIN(X(J))*(CI*T9(J)*DX/2.0D00+C)
   19 W(J)=R/(E*T(J))*(NHOOP(J)-POIS*NPHI(J))-UPHI(J)*CT(J)
C
C  XF, YF ARE THE COORDINATES OF THE MIDDLE SURFACE AFTER DEFORMATION.
C
      DO 20 I=1,INP1
      XF(I)=XI(I)+(-UPHI(I)*DCOS(X(I))+W(I)*DSIN(X(I)))
   20 YF(I)=YI(I)+(UPHI(I)*DSIN(X(I))+W(I)*DCOS(X(I)))
C
C
C     WRITE(6,100) (DEG(I),QPHI(I),NPHI(I),NHOOP(I), I=1,101)
C     WRITE(6,120) (DEG(I),MPHI(I), MHOOP(I), I=1,101)
C     WRITE(6,100) (DEG(I),B(I),KPHI(I),KHOOP(I),I=1,101)
C     WRITE(6,120) (DEG(I),UPHI(I),W(I),I=1,101)
      WRITE(6,100) (XI(I),YI(I),XF(I),YF(I),I=1,101)
  100 FORMAT(//101(4(5X,E14.7)/)///)
C 120 FORMAT(//101(3(5X,E14.7)/)///)
      RETURN
      END
C$ENTRY
```

BIBLIOGRAPHY

1. Augusteyn, R. C., H. B. Collins, and K. M.Rodgers. The Eye: Volume 1. St. Albans, VT: Eden Press, Inc., 1979.

2. Bores, Leo D., William Myers, and John Cowden, "Radial Keratotomy: An Analysis of the American Experience," Annals of Ophthalmology. 13(8): 941-948, August 1981.

3. Bergmann, Stephen and M. Hetenyi, "Analysis of Spherical Shells of Variable Wall Thickness," Journal of Applied Mechanics. 7: 88-89, June 1940.

4. Calkins, Joseph L., Bernard F. Hocheimer, and Walter J. Start, "Corneal Wound Healing: Holographic Stress-Test Analysis," Investigative Ophthalmology and Visual Science. 21(2): 322-334, 1981.

5. Collins, Richard and Terry J. van der Werff. Mathematical Models of the Dynamics of the Human Eye New York: Springer-Verlag, 1980.

6. Davson, Hugh. Physiology of the Eye. New York: Churchill Livingstone, 1980.

7. Duke-Elder, Sir Stewart, ed. System of Ophthalmology: Volume 2, The Anatomy of the Visual System. London: Henry Kimpton, 1976.

8. Duke-Elder, Sir Stewart, ed. System of Ophthalmology: Volume 8, Diseases of the Outer Eye, Part 2. London: Henry Kimpton, 1977.

9. Dunphy, Edwin B., "The Biology of Myopia," New England Journal of Medicine. 283(15): 796-800, October 8, 1970.

10. Fatt, Irving. Physiology of the Eye: An Introduction to the Vegetative Functions Boston: Butterworths, 1978.

11. Fischer, Ladislav. Theory and Practice of Shell Structures. Berlin: Wilhelm Ernest and Sohn, 1968.

12. Flugge, Wilhelm. Stesses in Shells. New York: Springer-Verlag, 1973.

13. Francois, J. and V. Victoria-Troncoso, "Molecular Biology of the Cornea," Sixth Congress of the European Society of

Ophthalmology: The Cornea in Health and Disease. Number 4: 29-39, 1981.

14. Fung, Y. C. Biomechanics: Properties of Living Tissue . New York: Springer-Verlag, 1981.

15. Girard, Louis J. Corneal Surgery. St. Louis: The C. V. Mosby Company, 1981.

16. Graebel, W. P. and G. W. H. M. van Alpen, "The Elasticity of Sclera and Choroid of the Human Eye, and Its Implication Scleral Rigidity and Accomodation," Journal of Biomedical Engineering. 99(4): 203-208, 1977.

17. Guyton, Arthur C. Textbook of Medical Physiology. Philadelphia: W. B. Saunders Company, 1980.

18. Hedbys, Bengt, "Corneal Healing," Sixth Congress of the European Society of Ophthalmology: The Cornea in Health and Disease. Number 4: 55-62, 1981.

19. Hoffer, Kenneth J., et al., "UCLA Clinical Trial of Radial Keratotomy: Preliminary Report," Ophthalmology. 88(8): 729-736, August 1981.

20. Hollister, S. C., "Stresses in Symmetrically Loaded Hemispherical Shells Having Tapered Edges," Journal of Applied Mechanics. 4(1): 11-15, March 1937.

21. Jester, James V., Richard A. Villasenor, and Janet Miyashiro, "Epithelial Inclusion Cysts Following Radial Keratotomy," Archives of Ophthalmology. 101: 611-615, April 1983.

22. Katz, Jeffrey I. and Herbert E. Kaufman, "Effects of Ocular Surgery on the Endothelium," p. 20-27 in Herbert E. Kaufman and Thom J. Zimmermann, eds. Current Concepts in Opthalmology: Volume 6. St. Louis: The C. V. Mosby Company, 1979.

23. Kobayashi, A. S., M. D. Larson, and A. F. Emery, "Reevaluation of Woo's Corneal and Sclera Data," 1977 Advances in Bioengineering. p. 41-42.

24. Kobayashi, A. S., L. G. Staberg, and W. A. Schlegel, "Viscoelastic Properties of Human Cornea," Experimental Mechanics. 13(12): 497-503, 1973.

25. Kobayashi, A. S., S. L-Y. Woo, C. Lawrence, and W. A. Schlegel, "Analysis of the Corneo-Scleral Shell by Method of Direct Stiffness," Journal of Biomechanics. 4: 323-330, 1971.

26. Kramer, Stephen G., "An Assessment of Radial Keratotomy," American Journal of Ophthalmology. 92(2): 286-295, 1981.

27. Kraus, Harry. Thin Elastic Shells. New York: John Wiley and Sons, Inc., 1967.

28. Leebovitch, Larry S. and Sheldon Weinbaum, "A Model of Epithelial Water Transport: The Corneal Epithelium," Biophysics Journal. 35:315-338, August 1981.

29. Le Grand, S. G. Physiologic Optics. New York: Springer-Verlag, 1980.

30. Lerman, Sidney. Radiant Energy and the Eye. New York: Macmillan Publishing Co., Inc., 1980.

31. McDevitt, David S. Cell Biology of the Eye. New York: Academic Press, 1982.

32. Miller, David and Jeffrey N. Weiss, "The Effect of Corneal Stretch on Endothelium," Ophthalmic Surgery. 12(10): 731-736, October 1981.

33. Mow, C. C., "A Theoretical Model of the Cornea for Use in Studies of Tonometry," Bulletin of Mathmatical Biophysics. 30: 437-453, 1968.

34. Newell, Frank W. and J. Terry Ernest. Ophthalmology: Principles and Concepts. St. Louis: The C. V. Mosby Company, 1974.

35. Nyquist, Gerald W., "Rheology of the Cornea: Experimental Techniques and Results," Experimental Eye Research. 7: 183-188, 1968.

36. Reddy, P. Ranga, "Russian Technique of Myopic Surgery," Indian Journal of Ophthalmolgy. 29:239-295, October 1981.

37. Rosenberg, L. C., "Structure of Connective Tissue Macromolecules," Human Joints and Their Artificial Replacements. Springfield, IL: Peter S. Water, Charles C. Thomas, Publisher, 1977.

38. Schachar, Ronald A., Truman D. Black, and Tseng Huang. Understanding Radial Keratotmy. Denison, TX: LAL Publishing, 1981.

39. Schachar, Ronald A., Norman S. Levy, and Les Schachar, eds. Keratorefraction. Denison, TX: LAL Publishing, 1980.

40. Schachar, Ronald A., Norman S. Levy, and Les Schachar, eds. Refractive Modulation of the Cornea. Denison, TX: LAL Publishing, 1981.

41. Schwartz, N. J., R. S. Mackay, and J. L. Sackman, "A Theoretical and Experimental Study of the Mechanical Behavior of the Cornea with Application to the Measurement of Intraocular Pressure," Bulletin of Mathematical Biophysics . 28(185): 585-643, 1966.

42. Spotts, Merhyle F., "Analysis of Spherical Shells of Variable Wall Thickness," Journal of Applied Mechanics. 6: 97-107, September 1939.

43. Timoshenko, S. P. and J. M. Gere. Theory of Elastic Stability. New York: McGraw-Hill Book Company, 1961.

44. Timoshenko, S. P. and S. Woinowsky-Krieger. Theory of Plates and Shells. New York: McGraw-Hill Book Company, 1959.

45. Villasenor, Richard A., James Salz, Douglas Steel, and Michael a. Krasnow, "Changes in Corneal Thickness During Radial Keratotomy," Ophthalmic Surgery. 12(5): 341-342, May 1981.

46. Von Rosenberg, Dale U. Methods of the Numerical Solution of Partial Differential Equations. New York: American Elsevier Publishing Company, Inc., 1969.

47. Waring, G. O., et al., "Rationale for and Design of the National Eye Institute Prospective Evaluation of Radial Keratotomy (PERK) Study," Ophthalmology. 90(1): 40-58, January 1983.

48. Wertenbacker, Lael. The Eye: Window to the World. Washington, D.C.: U.S. News Books, 1981.

49. Woo, S. L-Y., A. S. Kobayashi, C. Lawrence, and W. A. Schlegel, "Mathematical Model of the Corneo-Scleral Shell as Applied to Intraocular Pressure-Volume Relations and Applanation Tonometry," Annals of Biomedical Engineering. 1: 87-98, 1972.

50. Yamada, Hiroshi, ed. Strength of Biological Materials. Huntington, NY: Robert E. Krieger Publishing Company, 1973.

51. Yamaguchi, Tatsuo, Frank w. Polack, John Valent, and Herbert E. Kaufman, "Endothelial Damage After Anterior Radial Keratotomy," Archives of Ophthalmology. 99: 2151-2158, December 1981.

The three page vita has been removed from the scanned document. Page 1 of 3

The three page vita has been removed from the scanned document. Page 2 of 3

The three page vita has been removed from the scanned document. Page 3 of 3